Cyclometallated iridium-carbazole complexes for OLED applications

Moore, Tom

CYCLOMETALLATED IRIDIUM-CARBAZOLE COMPLEXES FOR OLED APPLICATIONS

TOM MOORE B.SC. (HONS) DUNELM

COLLINGWOOD COLLEGE

DEPARTMENT OF CHEMISTRY

UNIVERSITY OF DURHAM

A THESIS SUBMITTED FOR THE DEGREE OF MASTER OF SCIENCE AT THE UNIVERSITY OF DURHAM

DECEMBER 2008

Declaration

The work described in this thesis was carried out in the Department of Chemistry at the University of Durham between September 2007 and August 2008. This thesis is the work of the author unless otherwise stated and has not been submitted for any other degree.

Copyright

Table of Contents

Abstract

Organic Light Emitting Diodes (OLEDs) are a relatively new multi-disciplinary research area. Much of the interest generated by OLEDs is due to their commercial potential as market leaders in display technology and ambient lighting solutions. The advancement of materials used in OLED devices has driven synthetic chemists to produce a great variety of structures for use in devices. Current phosphorescent triplet emitters are based on heavy metal complexes either as a single unit or incorporated into a polymer backbone.

This work presents the synthesis of ligands via a Suzuki cross-coupling methodology and their subsequent homoleptic tris-cyclometalated iridium complexes. Ligands are based on a carbazole-pyridyl structure with a substituent group on the pyridyl aimed at tuning the complexes' HOMO-LUMO gap to produce different wavelengths of emission. Several new synthetic strategies were employed in an attempt to simplify the synthesis of the ligands although it was found that the most efficient method was the original synthesis of these ligands as performed in the Bryce group. An electron donating group (EDG) or an electron withdrawing group (EWG) was added in attempts to blue shift or red shift the emission, respectively. The complexes are based on two parent systems (shown below) which give two series of functionalised complexes.

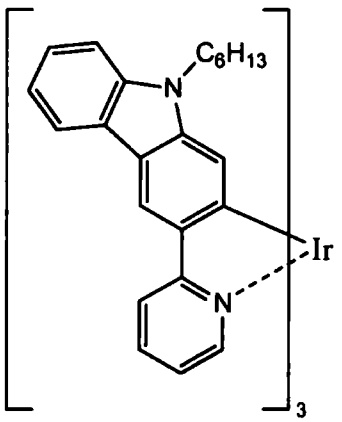

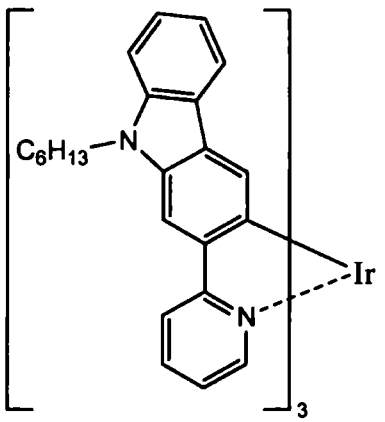

Investigations were carried out into the photophysical properties of these phosphorescent triplet emitters to determine the extent to which the functionalisation altered the emission properties. Solution state phosphorescence emission studies demonstrated that the substituent EDG and EWG groups had a significant effect over the emission of the complex with shifts up to 54 nm within a series and a total range of emission covering between 504 and 637 nm; green to red emission. Solution cyclic voltammetric data are also reported.

TD-DFT computations concurred with the current theories regarding the excited state of such complexes, in that the emission was occurring from a mixed MLCT/π-π^* transition. Preliminary device investigations demonstrated relatively low external quantum efficiencies due to a number of factors. It was also determined that the substituent group had a significant effect in shifting electroluminescence emission.

Acknowledgements

Firstly I would like to thank Professor Martin Bryce for his supervision, support, encouragement and most of all contagious enthusiasm for the subject. Without this, my interest would not have been sparked in this field, this thesis would not have been written and the work not performed, so thank you.

Our lab was always an enjoyable place to work, made so by the other people in the group. I thank them for their welcoming attitude, their passed on knowledge, help and friendship. Life in the lab would certainly have been much duller without them.

If you are a student in the Bryce group of the present then I wish you luck. It's worth it. Oh, and try not to touch the container marked 'explosive'. I jest, but really, do handle with care.

My thanks go also to the members of the analytical staff at the department whose expert knowledge aided me in identifying and characterising the compounds presented here. In particular the NMR staff who permitted my samples to occasionally monopolise their machines.

I thank Dr. Hameed Al-Attar in physics for his work in fabricated devices based on my complexes and he even let me keep one. His work and explanations of all things 'physicsy' was greatly appreciated. Equally appreciated was the work of Dr. Mark Fox in his computations, I thank him for this and the four thousand words he helped me not to write.

This year, my fourth in Durham, was made all the more enjoyable by friends both within and outside the department. Working in the department and living in college just wouldn't have been the same without them.

Finally I would like to thank my parents for their belief, encouragement and support throughout my years at Durham. Thank you.

Chapter 1 – An Introduction to Organic Light Emitting Diodes

This chapter aims to give the reader an overview of the important features of Organic Light Emitting Diodes (OLEDs). The chapter will define what an OLED is, what sort of materials go into making an OLED and the mechanisms by which they work. This will include a brief history of the existing and potential applications of OLEDs and the development of the materials that make this possible.

Firstly it is important to define what exactly an Organic Light Emitting Diode is. The simplest definition of an OLED would be an electroluminescent organic material sandwiched in between two electrodes to produce light; this will be examined later in device structure. Applications for OLEDs include ambient lighting and use in display screens for electronic devices.

Current ambient lighting solutions are not ideal, for example, a tungsten filament bulb only emits 10% of the energy consumed as light, the rest is emitted as heat. This leads to a poor efficiency of approximately 15 lmW^{-1} and operational lifetimes of about 1000 hours. Recent advances in lighting have introduced 'energy efficient' (fluorescent) light bulbs which have increased efficiency to approximately 60 lmW^{-1} and lifetimes of more than three times that of the traditional filament bulb. Fluorescent lighting is more efficient than filament bulbs but is also more costly and there are environmental drawbacks as most fluorescent bulbs contain mercury. The standard in ambient lighting comes from this fluorescent bulb, which OLEDs must surpass, or at the very least compete with, on a performance and cost efficient basis if they are to succeed as ambient lighting sources.

Solid state lighting (both organic and inorganic LEDs) is increasingly being used instead of other light sources for ambient lighting applications. Everyday examples of this can be seen in the taillights of buses or in traffic lights where LEDs have replaced the traditional filament bulb. OLEDs have been demonstrated to be more efficient and have greater lifetimes than fluorescent bulbs which in the future should lead to a greater inclusion of OLEDs in everyday lighting applications.

An application in which OLEDs excel is information displays. The traditional Cathode Ray Tube (CRT) display has existed for over a century and in recent decades has slowly been replaced by the plasma display and Liquid Crystal Display (LCD). Advantages in these displays include a large reduction in volume required for the same surface area display, *i.e.* plasma and LCDs are 'flat screen'. Disadvantages include the increased cost of production which is passed onto the consumer; the displays can also exhibit 'screen burn' where an image is burnt onto the display through excessive use of an unchanging image; LCDs require a backlight to provide the lighting source as the liquid crystals simply provide the red, green and blue pixels required to make a 'full colour' display.

The backlight leads to poor contrast ratios of *ca.* 1,000:1, brightness levels are also approximately 300 cd/m^2.

In contrast, OLEDs do not require a backlight as it is the actual organic material that is emitting the red, green or blue light that makes up a pixel. Aside from leading to much greater contrast ratios (*ca.* 1,000,000:1) the lack of a backlight means the display can be much thinner. OLED displays have even been fabricated on flexible substrates with good results, although often with poorer lifetimes due to the non-hermetically sealed display which degrades through contact with moisture and oxygen in the air.

The first full colour active matrix OLED (AMOLED) display was commercialised in 2003 with its incorporation into a digital camera. This represented the first inclusion of an OLED display into a small electronic device. Practically every type of electronic device which requires a small display screen has now used an OLED display at some point. The expectation that an OLED TV would be commercialised came to fruition in 2008 when Sony announced the first OLED TV, the XEL-1. Although the screen is relatively small in TV terms (it measures 11 inches diagonally) it represented a leap forward in the commercialisation of OLEDs. The Sony XEL-1 offers a contrast ratio of >1,000,000:1, high brightness and a viewing angle of 178°. Representative images of the products can be seen below in Figure 1.

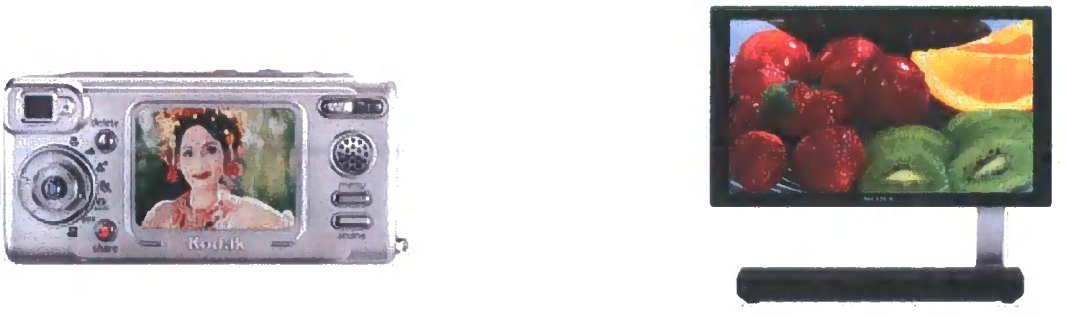

Figure 1 - First examples of OLED displays

The increasing use of OLED displays in products such as these has lead to the increase in market value of OLEDs. Although estimates vary the worldwide market value of OLEDs is currently worth *ca.* £250m with an expectation that this will rise to over £2b by 2010[1]. A variety of companies are currently involved in OLED technologies leading to an accelerating pace of advances in the field and products appearing on the shelves for the benefit of the end users.

1.1 Luminescence

Luminescence is the production of light from a compound, either organic or inorganic. Luminescence can occur following a number of different mechanisms. Organic compounds suitable for OLED applications will display photoluminescence and electroluminescence which will be explained in detail below.

In order for a material to emit light it needs to be in a higher energy (excited) state which can convert to the ground state through the release of energy in the form of a photon or through a non-radiative pathway. These excited states can be formed by photoexcitation (photoluminescence) or electronic excitation (electroluminescence).

1.1.1 Photoluminescence

In photoluminescence an incident photon excites an electron from the highest occupied molecular orbital (HOMO) to the lowest unoccupied molecular orbital (LUMO). A molecular excited state is formed from which the electron can then decay back to the HOMO. This process can be radiative or non-radiative, *i.e.* a photon can be released or a non-radiative process can aid the relaxation of the electron to the HOMO. The energy of the photon will be equal to the energy difference between the HOMO and LUMO. A schematic of photoluminescence can be seen in Figure 2 below.

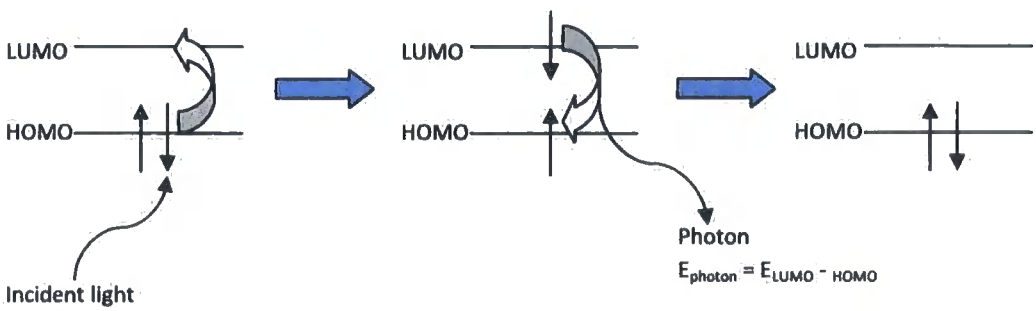

Figure 2 – Photoluminescence schematic

1.1.2 Electroluminescence

Electroluminescence can be defined as the production of light from a material when an electric field is applied across it. It requires the excitation of the material into a higher energy state which can

occur through various mechanisms and the subsequent relaxation of the material to a lower energy state resulting in the release of a photon. Long before organic materials were thought of as potential electroluminescent materials inorganic semiconductors were being used in light emitting diodes - LEDs

The first example of electroluminescence was reported over 100 years ago[2] in a note to the editors of *Electrical World*. It was found that when a potential difference was applied across a crystal of carborundum (silicon carbide) a yellowish light was produced. Unfortunately, the discovery was not followed up and it was not until the mid-1920s that the LED was 're-invented'[3].

When an electric field is applied across an inorganic LED charges are injected at the electrodes; the charge flows from the p-side to the n-side, which can be regarded as charge flowing from the anode to the cathode. The semiconducting material is doped with impurities which create a p-n junction where opposite charges recombine and relax to a lower energy state producing a photon. This mechanism of electroluminescence is called recombination and is also the primary mechanism by which organic electroluminescent materials produce light.

1.1.2.1 Organic Electroluminescence

Organic electroluminescence is the electronic excitation of organic compounds to emit light. To do this electrons are injected from the cathode into the LUMO and removed from the HOMO to the anode. This forms radical anions with an electron (negatively charged) on the LUMO and radical cations with a hole (positively charged) on the HOMO (Figure 3).

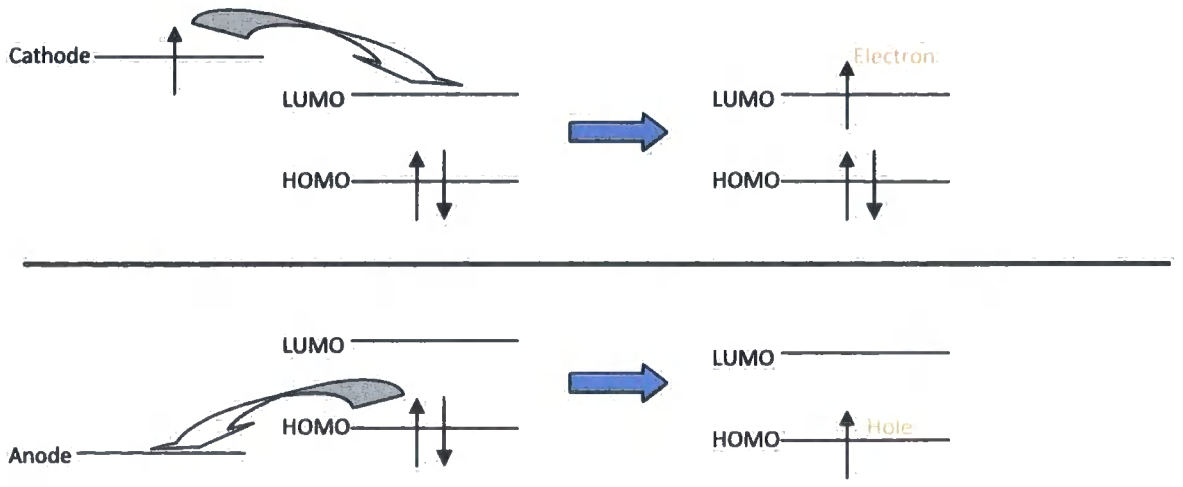

Figure 3 – Electron and hole formation

These charges migrate within the organic material through a 'hopping' mechanism (*vide infra*). If the charges combine within the emissive material they can form a molecular excited state. These excited states are called 'excitons' and are the emissive states that can release photons to decay to the ground state (Figure 4).

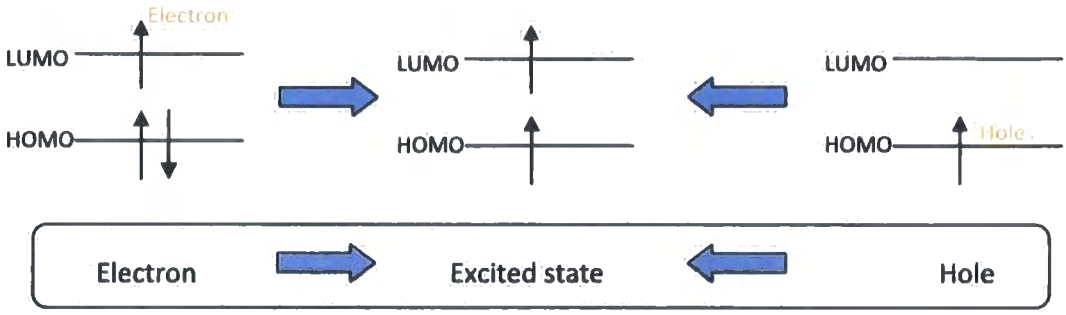

Figure 4 – Exciton formation

The total spin of the exciton can either be S=0 or S=1. The associated spin multiplicity (using 2S+1) of S=0 is 1 and of S=1 is 3 hence these states are called singlets and triplets. With a total of 4 states and an equal chance of forming each state the probability of forming a singlet or triplet exciton is 25% and 75%, respectively. The singlet to triplet ratio has been measured experimentally[4] and found to be within experimental limits of the expected 25:75, although more recent work suggests that in some polymeric materials a higher ratio of singlets can be generated[5].

Electrons can quickly and easily decay from singlet excitons to the ground state (HOMO) which can release a photon in a process called fluorescence. Alternatively, the electron can decay slowly from the triplet exciton to the ground state with the release of a photon – this is called phosphorescence. If the molecule has been excited electronically these terms are referred to as electrofluorescence and electrophosphorescence. The lifetimes of fluorescence and phosphorescence are very different with fluorescence being a much faster process relative to phosphorescence. This is because of the allowed and forbidden nature of fluorescence and phosphorescence, respectively. In fluorescence the decay of an electron from the exciton to the ground state is 'allowed' by Pauli's exclusion principle which states that no two identical fermions can occupy the same quantum state simultaneously. Hence the decay of an electron from a singlet exciton in which the electron's spin is paired is allowed, whereas the comparable decay from a triplet exciton in which the electron's spin is unpaired is not allowed. Due to the forbidden transition from a triplet exciton the probability is very low and for most materials this does not occur very often. The energy of a triplet exciton is lower than the energy of a singlet exciton due to the reduced repulsion of the electrons. To allow this decay from the triplet exciton a mixing of the singlet and triplet states occurs and the excited electron will transfer to the lower triplet excited state. This

process known as intersystem crossing (ISC) results in a triplet state with partial singlet character making the transition to the ground state possible. This results in a red shift in emission as the electron is decaying from a lower energy state, hence the gap between the excited state and the ground state is lower and according to E=hν the wavelength of the emitted photon will be longer. Phosphorescent materials that are suited for OLED applications will almost exclusively emit from the triplet exciton leading to very high efficiencies and helping ensure colour purity of the emitted light.

In an OLED device the phosphorescent material will usually be dispersed within a charge transport layer. The phosphorescent material is often referred to as the guest and the charge transport layer as the host. When the absorption spectrum of the guest overlaps with the emission spectrum of the host efficient transfer of excitons between the two can occur. An efficient transfer of singlet and triplet excitons should occur between host and guest as it is the latter that should exclusively emit within the device. Förster transfer (also called induced dipole transfer) can be used to explain the transfer of singlet excitons between the host and guest. However, if Förster transfer occurs along with the electron exchange between the host and guest (Marcus/Dexter transfer, Figure 5) then triplet excitons can also be transferred as the total spin of the system is conserved. Förster transfer occurs over relatively large distances of ~100 Å, whereas Marcus transfer occurs over shorter distances of ~ 10 Å, hence the transfer of triplet excitons can only occur over these relatively short distances where both processes can happen simultaneously. This means that the transfer of both singlet and triplet excitons from the host to the guest can excite phosphorescence.

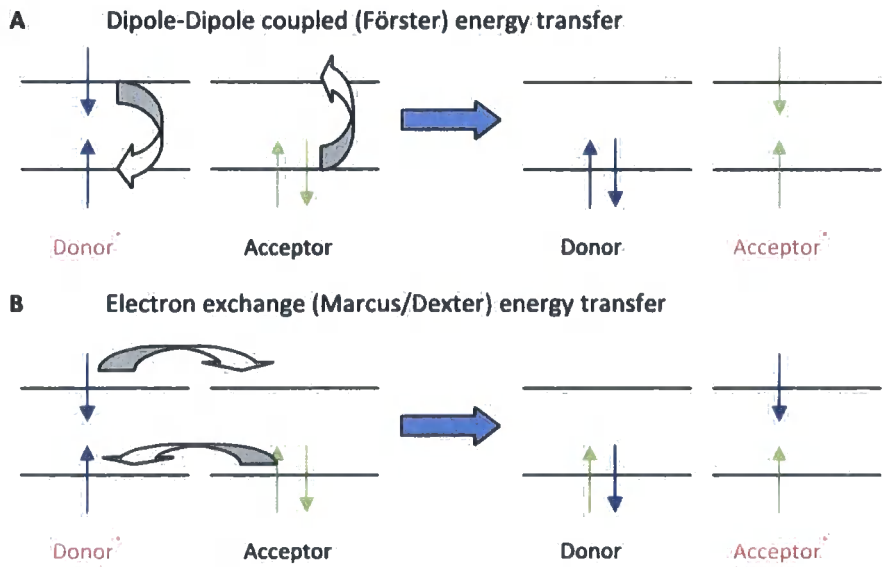

Figure 5 – A schematic of Förster energy transfer (A) and Marcus energy transfer (B); reproduced from [22]

It is often found that there is an optimum amount of doping of the phosphorescent guest in the host material[6]. With too little phosphorescent dopant saturation ('concentration quenching') can occur

due to the long lifetimes of phosphorescent excitons. If this occurs and the host is able to emit, emission will be observed from the host, which is likely to result in a hypsochromic (blue) shift in device emission as the host is likely to have higher energy emission. With an excess of phosphorescent dopant triplet-triplet annihilation can occur resulting in the reduction of triplet excitons. In triplet-triplet annihilation the total spin of the system is conserved when two triplet excitons combine and form a singlet exciton and singlet ground state (Figure 6).

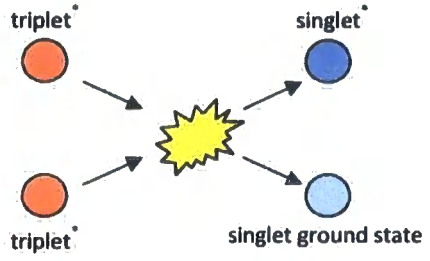

Figure 6 – Triplet-triplet annihilation

1.2 Device Structure

In order for an electroluminescent material to emit light it is placed between two electrodes. Early examples used single crystals, *e.g.* anthracene as the emissive material. A significant development upon this method was the use of thin films (initially of anthracene) which dramatically reduced the voltage required to produce electroluminescence (often referred to as the drive or turn-on voltage)[7]. The organic emissive layer usually forms an amorphous film between the cathode and the anode. The cathode is typically a metal electrode (*e.g.* Al/Ba or Mg:Ag alloy) with a low work function to promote the injection of electrons into the device. The anode is usually indium-tin-oxide (ITO) - a material that is transparent to the emitted light, although thin films of Au have been used in the past as the anode; these materials exhibit a high work function to promote the injection of holes into the device. It is therefore possible to fabricate a device using only three layers – Cathode/Emissive layer/Anode. It is not usual to count the cathode and anode as layers, so this type of device is usually referred to as a single layer type. (Figure 7).

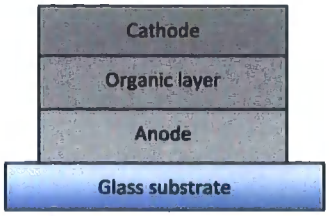

Figure 7 – Schematic diagram of a single layer OLED

When an electric field is applied holes and electrons are generated at the anode and cathode respectively and migrate towards each other with the possibility of forming excitons when they meet in the organic layer. Adding an extra layer to the device that is complementary to the transporting properties of the emissive material can improve device efficiency. These layers are called electron or hole transporting layers (ETL and HTL). In 1987 Tang and VanSlyke were the first to introduce one of these layers into a device[8] initiating a revolution in the efficiency of OLEDs. These devices can come in several configurations, categorised as two-, three- or multi-layer devices. Two layer devices consist of a HTL and an ETL where one layer is the emissive material (Cathode/ETL/HTL/Anode). Alternatively three layer devices consist of a HTL and ETL plus a separate emissive layer (Cathode/ETL/Emissive layer/HTL/Anode). Certain properties of HTLs and ETLs are alike, such as the ability to transport charge effectively across the layer. Thermal stability and the capability of forming defect free films are also properties of proficient HTL and ETLs. HTLs should possess a low solid state ionisation potential and a low electron affinity (*i.e.* the ability to form cations easily) whereas ETLs possess the converse properties (form anions easily). This also means that both ETLs and HTLs should be good at blocking the opposite charge, for example, a HTL should transport holes but block electrons. This helps confine the charges in the emitting layer and improves the chances of exciton formation and consequent emission with good efficiency.

A classic ETL material (used by Tang and VanSlyke) and one that is still in use today is tris(quinolin-8-olato) aluminium - Alq_3, the structure of which is seen below.

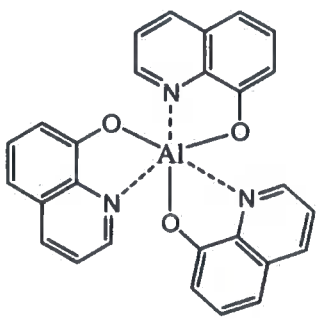

Alq_3 (1)

Variants of Alq_3 have also been used successfully as ETL materials to improve device performance, such as $Almq_3$[9] where an extra methyl group is added.

The HTL material in the Tang and VanSlyke device was a diamine, TAPC (**2**). Diamines are very common as HTL materials and many have similar structures to TAPC with multiple phenyl groups and a biphenyl linker between the amines such as *N,N'*-diphenyl-*N,N'*-bis(3-methylphenyl)-1,1'-biphenyl-4,4'-diamine, TPD (**3**)[10].

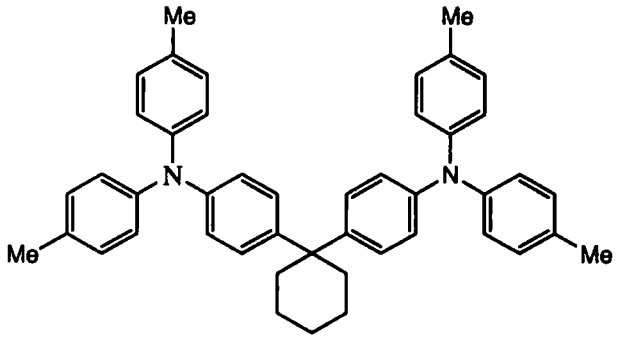

TAPC (**2**)

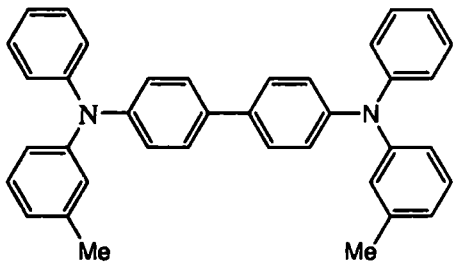

TPD (**3**)

Other diamine HTL materials have been synthesised and utilised in devices such as a TPD derivative NPB[11], where each amine has a naphthyl unit instead of the tolyl present in TPD. Both TPD and other diamine materials make good HTLs because of their strong hole transporting abilities and electron blocking properties.

1.2.1 Device Comparison

To compare devices we must define several criteria that are suitable for this purpose.

Devices operate when an electric field is generated by applying a potential difference (voltage) between the two electrodes. At a certain voltage the energy barriers for emission will be overcome and the device will start to emit light, this is known as the drive or turn-on voltage. The lower the drive voltage the better, as a high drive voltage can lead to an increase in temperature of the emissive material and degradation.

An important criterion for device performance is efficiency, both internal and external quantum efficiency. Efficiency can be explained in simple terms as follows - for each pair of charges that is injected into the device an exciton can be formed and from each exciton a photon can be emitted in the relaxation to the ground state. Ideally the ratios of these events will be 1:1, giving 100% internal quantum efficiency. Unfortunately, this does not translate into 100% external quantum efficiency

due to device limitations. The formation of an exciton does not guarantee that a photon can be observed from the device. This is the first of several chance processes that must all occur in order for a photon to be emitted from the device. Indeed, the injection of an electron and hole into the device does not guarantee that an exciton is formed. When an exciton is formed it must decay radiatively, releasing a photon within the device. This is internal emittance and is measured through internal quantum efficiency. Provided the photon is not absorbed internally it can be emitted externally, leading to external quantum efficiency.

A further performance indicator is the brightness or luminance that a device produces. Results are often reported at high voltages which could not be maintained during normal device use. This leads to another property of devices, lifetime. If a device is to be used in a commercial product such as an OLED TV the lifetime must match or exceed that of current products. It is often found that devices producing high energy emission (blue) have shorter lifetimes than those producing low energy emission (red) due to degradation of the higher bandgap material.

1.3 Organic Materials

Organic Materials can either be small molecule or polymeric. This short review will focus on small molecules as they are of relevance to the work reported later. For completion it is noted that fluorescent polymer light emitting devices, PLEDs, have had a huge impact in the field of OLEDs since the discovery of electroluminescence in a poly(phenylenevinylene) (PPV) derivative[12].

Small molecule organic materials for LEDs can be classified into two families – fluorescent and phosphorescent emitters.

1.3.1 Fluorescent Emitters

Early OLED work focused on organic fluorescent emitters and in particular single crystals as the organic electroluminescent (EL) material. In 1965 Helfrich and Schneider[13] used anthracene single crystals to produce blue electroluminescence using aqueous based electrodes. Improving the charge injection on previous work[14, 15] they used aqueous electrodes of cationic and anionic anthracene produced through the reaction with $AlCl_3$ and metallic sodium, respectively, although these electrodes were used in separate devices. Prior to this work, electron injection into anthracene had not been observed. Interestingly, they noted a 'luminous zone' in the crystal close to the anode suggesting that the electrons were travelling rapidly within the material from the cathode to combine with holes near the anode forming excitons to produce the luminescence. They also

commented that although singlet and triplet excitons were expected to be formed through charge recombination, only the singlet states were emitting, noting that the triplet states were expected to decay through a non-radiative pathway.

Later developments would see the use of thin amorphous films as the organic layer, *e.g.* the anthracene films studied by Vincett *et al.*[7]. The film was produced by vacuum deposition, forming a 0.6 μm film of polycrystalline anthracene. It was found that the drive voltage was dramatically reduced to 30 V when viewed under ambient lighting conditions or as low as 12 V when the EL was viewed in a darkened room. Although the quantum efficiency of the devices was only ca. 0.05% this was the first time that EL had been observed at voltages significantly less than 100 V. It is important to reduce the drive voltage in order to reduce degradation and increase the lifetime of the organic material. Similar results were achieved for perylene (*vide infra*) and 1,12-benzperylene for which EL had not previously been observed.

It should be noted for completion that tetracene was also widely used both as single crystal and thin film devices[16], often in conjunction with anthracene.

In 1987 Tang and VanSlyke published a revolutionary paper[8] describing a two layer device of a metal chelate complex (Alq_3, **1**) as the electron transporting and emitting layer and a diamine (TAPC, **2**) as the hole transporting layer. The inclusion of these transporting layers was found to greatly improve the efficiency of the device. The device structure is shown in Figure 8.

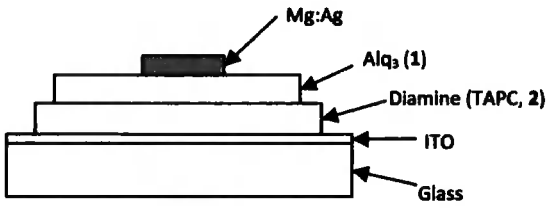

Figure 8 – Device structure reproduced from [8]

The films were deposited through vacuum deposition; the first organic layer on top of the ITO anode was a TAPC layer of *ca.* 750 Å thickness followed by layer of Alq_3 of *ca.* 600 Å thickness. The cathode was a Mg:Ag alloy with a composition of *ca.* 10:1 respectively. It was reported that the emission spectrum was identical to the photoluminescence spectrum of the Alq_3 thin film demonstrating that the Alq_3 layer is the emissive layer in the device and that the charge recombination was taking place exclusively in this layer. This work also demonstrated that the diamine TAPC is a unipolar transporting material, *i.e.* it transports only holes. The external quantum efficiency of the device was about 1%, a large improvement over the 0.05% reported by Vincett *et al.*[7] in one of the first reports

of thin film devices. The device has a drive voltage of about 6 V and can also produce a high brightness of >1000 cd/m^2 at a voltage of less than 10 V. When this is compared to Vincett's anthracene film drive voltage of 12 V and a darkened room required to observe the EL, it is clear this was a great improvement. To put 1000 cd/m^2 into perspective, a CRT TV will have a brightness of around 350 cd/m^2, easily seen under ambient lighting conditions.

It is noteworthy that an Alq_3 derivative, tris(4-methyl-8-quinolinolato)aluminium - $Almq_3$ was synthesised in 1997[9]. Using a very similar device structure to Tang and VanSlyke of ITO/**3** (TPD)/$Almq_3$/Mg:Ag this device produced an external quantum efficiency of 2.5% and a maximum luminance of 26000 cd/m^2 at 14 V, a good performance for an electrofluorescent based device.

The advances in 1987 spurned on efforts to create new hole- and electron-transporting materials to improve device performance. Adachi and co-workers[10] developed a three layer device utilising an aromatic diamine (TPD, **3**) as the HTL and a perylene tetracarboxylic acid derivative (PV) as the ETL. Anthracene, coronene and perylene (see below) were chosen as the emissive materials as they fluoresce with different colours.

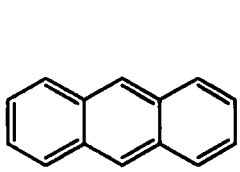

Anthracene (**4**)

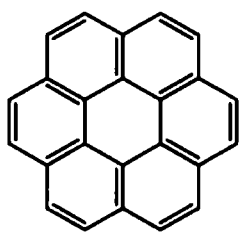

Coronene (**5**)

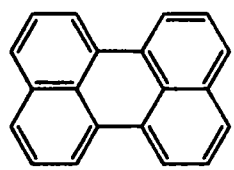

Perylene (**6**)

This work furthered the use of diamines as the HTL:TPD has a similar structure to TAPC originally used in Tang and VanSlyke's two-layer device[8] (*vide supra*). The ETL of a perylene tetracarboxylic acid derivative (PV) took electron transporting materials in a new direction, moving away from the metal chelate complex. The HTL and ETL layers both consist of unipolar transport materials ensuring charge recombination takes place in the emitter layer. Hence, the device emission is tuneable based on the emitting material; EL peaks of 420, 500 and 600 nm were obtained for anthracene, coronene and perylene, respectively. It is noted in this paper that optimisation of the layer thickness in the devices had not been undertaken. The layer thicknesses were quite large when compared to Tang and VanSlyke's device with the TPD layer having a thickness of 2000 Å, and the emitting layer and PV layer having thicknesses of 1000 Å each resulting in the drive voltage being relatively high and emission visible at 50 V in a darkened room. Optimisation of the thicknesses of these layers could result in a lowering of the drive voltage and an increase in the efficiency of the device. Figure 9 shows the device structure.

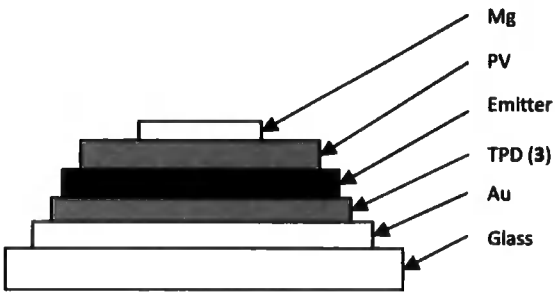

Figure 9 – Device structure reproduced from [10]

Adachi and co-workers[17] further developed their three layer device by testing different emitting materials. Several fluorescent dyes were examined before 12-phthaloperinone was chosen which emitted yellow (λ_{max} 580 nm) fluorescence at 60 V which was visible under ambient lighting conditions. The brightness of this material was reported to be approximately 400 times larger than that of the device when perylene was used as the emissive material. Hence, the choice of the organic emissive material was established as crucial to the effectiveness of the device it produces.

In 1989 Tang, VanSlyke and Chen[18] published a novel device structure based on their original two layer device. This new structure used a fluorescent dopant in the Alq_3 layer giving a device structure of ITO/diamine/Alq_3(**3**)/doped Alq_3/Alq_3(**3**)/Mg:Ag (Figure 10).

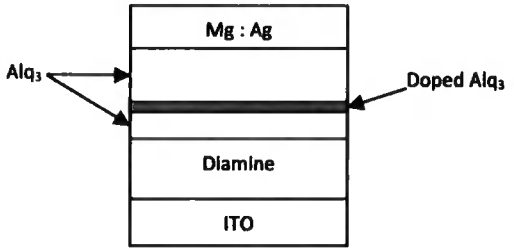

Figure 10 – Device structure reproduced from [18]

They noted that to achieve a higher efficiency they must use an emissive material with a higher fluorescence quantum efficiency than Alq_3 (8%). This would mean finding an electron transporting material as effective as Alq_3 but with better emissive properties or the alternative route of increasing the Alq_3 luminescence efficiency. To achieve this, a dopant was introduced into the Alq_3 layer. The dopants used were based on laser dyes - DCM1, DCM2 and Coumarin 540. It was found that this increased the fluorescence efficiency to as high as 40% compared with the undoped 8% of the pure Alq_3 emitter. At optimum concentrations of dopants the external quantum efficiency of the device was increased to *ca.* 2%, a doubling of the undoped Alq_3 device. This method produced tuneable

devices dependant on which dopant is used; a range of colours from blue-green to orange-red were produced in the work.

1.3.2 Phosphorescent Emitters

With fluorescent emitters' internal quantum efficiency effectively capped at 25% a new type of organic luminescent material was needed. The harvesting of both singlet and triplet states is necessary for increasing the efficiency of OLED devices. When a material exhibits this property under an induced electric field it is known as electrophosphorescence and leads to a theoretical 100% internal quantum efficiency.

The first example of electrophosphorescence was from benzophenone, reported in 1996[19]. The device used consisted of three layers with the benzophenone guest dispersed in a poly(methylmethacrylate) host. It was found that the phosphorescence emission was very weak at room temperature (273 K) but was prevalent at 100 K at the turn on voltage of *ca.* 17 V. This is due to poor intersystem crossing in benzophenone and non-radiative processes being the primary method of exciton decay at room temperature. No transfer of triplet excitons was found between the host polymer and the benzophenone making it unsuitable for OLED applications as this will hamper the efficiency of the device.

Another material that exhibits electrophosphorescence is 2,3,7,8,12,13,17,18-octaethyl-21H-23H-porphine platinum (II) (PtOEP, **7** - see below).

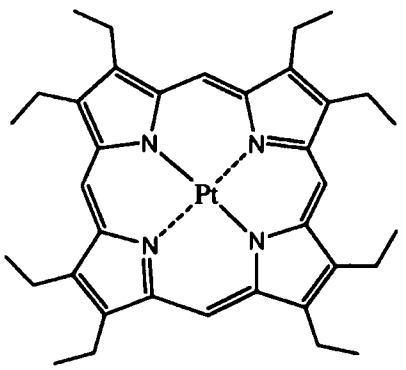

PtOEP (7)

The use of this material was investigated in 1998 by Baldo *et al.*[6] in an Alq_3 host using a multi-layer device. Alq_3 was chosen as its emission spectrum overlaps with PtOEP's absorption spectrum at 530 nm allowing efficient transfer of singlet excitons and giving a reasonable assumption that triplet excitons are likely to be transferred between host and guest. It was found that short range Marcus

transfer dominates over longer range Förster transfer in the transfer of excitons. Combining this with the fact that PtOEP has a relatively long exciton lifetime lead us to the proposal that saturation should occur with lower dopant concentrations. This was indeed observed (at approximately 1% dopant concentration) and was supported by the observation of increased Alq_3 emission at low concentrations. It can be alleviated by increasing the concentration of PtOEP which demonstrated that 6% was the optimum dopant concentration as maximum external and internal quantum efficiencies of 4% and 23% respectively were achieved with ≥90% energy transfer from Alq_3 to PtOEP occurring. This work demonstrated that both the singlet and triplet excitons participate in the energy transfer between the host and guest. Emission was not observed from the singlet state of PtOEP (*ca.* 580 nm) but was seen from the triplet state at 650 nm demonstrating the strong inter-system crossing within the material.

The inclusion of a metal centre into an organic ligand or chelate structure is a common method of increasing the efficiency of a material. The inclusion of Pt within the poryphine ring of PtOEP increases singlet-triplet mixing, *i.e.* the triplet state gains further singlet character and *vice versa* facilitating inter-system crossing and reducing the phosphorescence lifetime by increasing spin-orbit coupling. The efficiency of PtOEP is limited by the triplet energy of the host material. For example, PtOEP in polystyrene exhibits an internal quantum efficiency of 50%[20] where the triplets are confined more tightly than in Alq_3. A host material with a larger triplet energy helps confine the triplets on the PtOEP and hence increases efficiency.

1.4 Iridium Complexes

Iridium complexes are a recent generation of phosphorescent guests in OLEDs. Their octahedral d^6 configuration is attractive as it increases the crystal field stabilisation energy. The introduction of a heavy metal atom such as Ir into a complex increases spin orbit coupling which aids intersystem crossing - the mixing of singlet and triplet excited states necessary for efficient phosphorescence. Most Ir complexes are charge neutral although charged complexes do exist. This section will focus on the work most relevant to what will be presented later.

The most common oxidation state for iridium is Ir^{III}, in fact this is exclusively the oxidation state of iridium found in neutral complexes for OLEDs. To balance the charge three negatively charged ligands are cyclometalated onto the iridium centre forming an organometallic ring structure. C^N ligands are often used for this purpose where the C is the cyclometalating element. Iridium complexes are often either bis- or tris-cyclometalated, with two identical cyclometalating ligands and an ancillary ligand, or three identical cyclometalating ligands.

Several different configurations of complexes exist although all involve the cyclometalation of organic ligands to the iridium centre. Examples are shown in Figure 11.

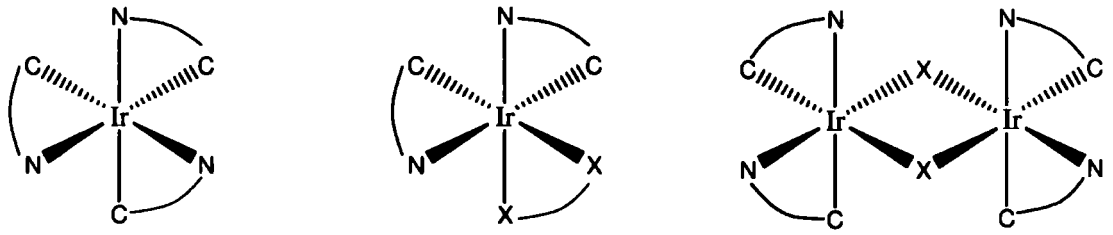

Figure 11 – Types of Iridium^{III} complexes

Iridium complexes exhibit a complex electronic structure[21]. Aside from the ligand centred excited states (LC) and metal centred excited states (MC) mixtures of the two occur. LC states involve the π bonding and π^* anti-bonding orbitals of the ligand where as MC states involve the d-orbitals of the metal. When there is an electron transferred to the ligands from the metal an excited state is formed known as a metal to ligand charge transfer state (MLCT). When the reverse occurs, the excited state is called a ligand to metal charge transfer state (LMCT). It is often difficult to determine the excited state or multiple excited states from which the complex is emissive, although this state is usually a mixture of LC and MLCT excited states. MLCT states exhibit stronger spin orbit coupling due to a larger overlap with the iridium which leads to an increase in ISC. The energy diagram for a high performance phosphor is shown in Figure 12.

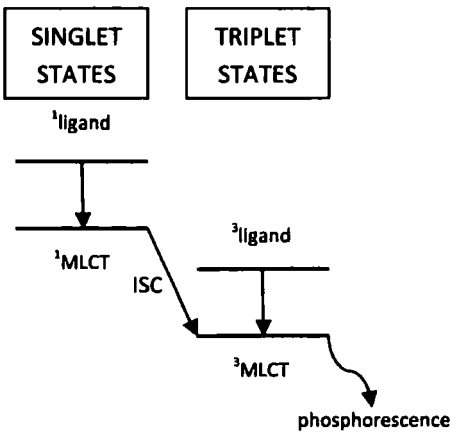

Figure 12 – An efficient phosphor, reproduced from [22]

In this schematic diagram it is the triplet MLCT excited state which is emissive although in a real complex it may be a mixture of the triplet ligand centred (π-π^*) and triplet MLCT excited states which emit.

1.4.1 *fac*-Ir(ppy)$_3$

Much of the current focus on iridium complexes in OLEDs can be traced back to *fac*-tris(2-phenylpyridine) iridium^{III} [*fac*-Ir(ppy)$_3$]. This complex utilising three C^N ligands in a facial configuration was synthesised by Baldo *et al.* in 1999 and used as a phosphorescent dopant in CBP[23]. The prototype device consisted of a transparent ITO anode with a 4,4'-bis[*N*-(1-napthyl)-*N*-phenyl-amino] biphenyl (α-NPD, a TPD derivative) hole transporting layer followed by the 4,4'-*N*,*N*'-dicarbazole-biphenyl (CBP, **9**) layer doped with *fac*-Ir(ppy)$_3$ (**8**) then a 2,9-dimethyl-4,7-diphenyl-1,10-phenanthroline or bathocuproine (BCP, **10**) layer, Alq$_3$ electron transporting layer and finally the Mg:Ag cathode (ITO/NPD/*fac*-Ir(ppy)$_3$(**8**) in CBP(**9**)/BCP(**10**)/Alq$_3$(**3**)/Mg:Ag), see below for the structures of *fac*-Ir(ppy)$_3$, CBP and BCP.

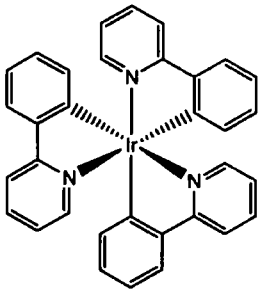

fac-Ir(ppy)$_3$ (**8**)

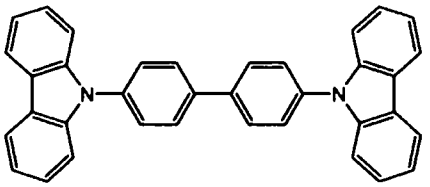

CBP (**9**)

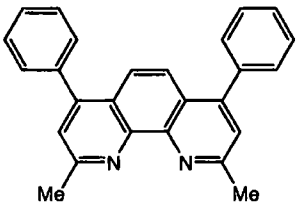

BCP (**10**)

Baldo *et al.* chose CBP as the host based on the assumption that although comparison of host emission and guest absorption spectra are reliable for the transfer of singlet states, they also have a bearing on the transfer of the important phosphorescent triplet states. CBP was a suitable host for PtOEP so was a logical choice for *fac*-Ir(ppy)$_3$ too.

The BCP layer used as an 'exciton blocking layer' was found to be particularly important for the performance of the device in confining excitons within the emitting doped CBP layer. The concentration of dopant was also crucial to the device performance as too low a concentration would lead to saturation, although the short phosphorescence lifetime of *fac*-Ir(ppy)$_3$ of *ca.* 1 μs means that lower concentrations can be used relative to other dopants with longer

phosphorescence lifetimes before saturation occurs. Figure 13 shows a comparison of dopant concentrations and different device structures.

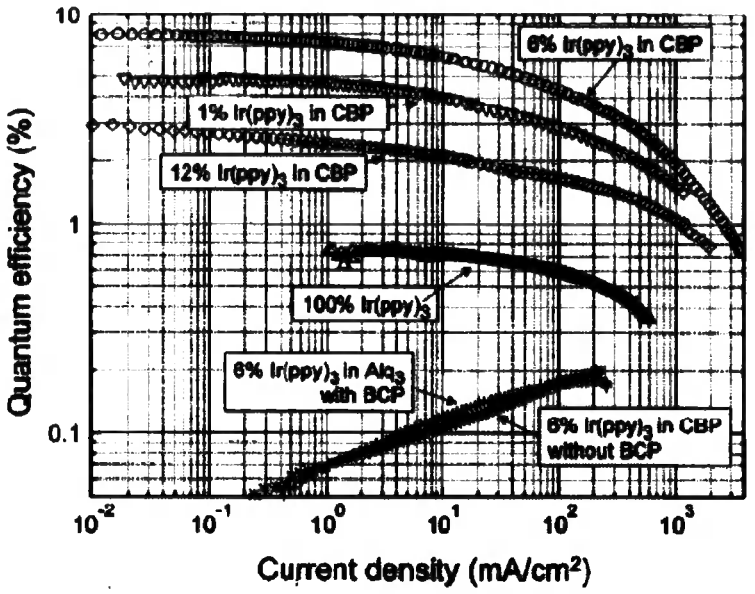

Figure 13 – A comparison of dopant concentrations and device structures with relation to EQE and current density. Copied from [23]

It is clear from Figure 13 that the optimum dopant concentration is 6% which gives an EQE of 8.0% at 10^{-2} mA/cm^2. The device performance was excellent for its time with peak power efficiency at 31 lm/W and a peak luminance of 100,000 cd/m^2. The λ_{max} of the EL from the device is 510 nm giving green light. Almost no EL is seen from CBP (λ_{max} = 400 nm) indicating that there is nearly complete energy transfer between the CBP host and iridium guest.

1.4.2 Functionalisation and Derivatives

The functionalisation of the ligand(s) around a heavy metal centre can lead to a shift in the EL emission of the complex[24]. The addition of either an electron withdrawing group (EWG) or electron donating group (EDG) will alter the position of the LUMO or HOMO of the complex affecting the wavelength of light emitted. To predict whether the wavelength will be red shifted (bathochromic shift) to lower energy or blue shifted (hypsochromic shift) to higher energy, density functional theory (DFT) calculations can determine the levels of the HOMO and LUMO; although theoretical calculations do not always correspond precisely to the experimental findings.

Grushin *et al.*[24] functionalised phenylpyridine ligands with a variety of different EWGs and EDGs and cyclometalated the ligands to an iridium centre. Aside from affecting the wavelength of

light produced, the efficiency and radiance of the device was also altered through the introduction of these groups. The groups were attached to either the phenyl or pyridyl rings (or to both) giving a series of *facial*-tris-cyclometalated iridium complexes as can be seen below.

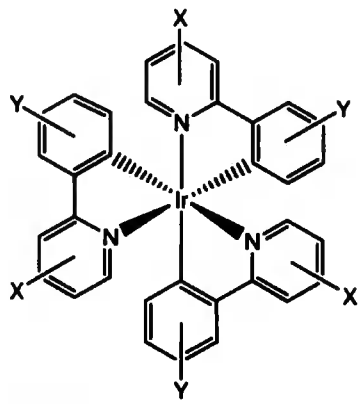

Table 1 showing the effects of placing groups X on the pyridyl and Y on the phenyl units of $Ir(ppy)_3$ derivatives.

X	*Y*	EL λ_{max}/nm	*Peak radiance cd/m²*
H	H	522	570
H	4-F	514	800
H	2-F	506, 526	1150
H	3-CF_3	517	1200
5-NO_2	3-CF_3	521, ≥630	7.6
5-CF_3	H	545	400
5-CF_3	3-CF_3	525	1500
5-CF_3	4-F	525	4800
5-CF_3	3-F	560	514
5-CF_3	2-F	525	340
5-CF_3	4-OMe	530, 563	175
5-CF_3	3-OMe	595	360
5-CF_3	4-OCF_3	520	411
3-Cl, 5-CF_3	H	575	190
3-(N), 5-CF_3	4-F	525	1500

Table 1 – The effect of substituent groups on the EL of $Ir(ppy)_3$

As shown in Table 1 a great variety of $Ir(ppy)_3$ derivatives were tested in OLED devices with peak performance of 4800 cd/m^2 achieved from the use of a CF_3 group in the 5-position on the phenyl and a F group in the 4-position of the pyridyl.

To explain the shift in emission due to the functionalisation of the ligand the HOMO/LUMO levels of the complex must be considered. Hay used DFT calculations to determine the densities and positions of the HOMO and LUMO on a 2-phenylpyridine iridium complex in 2002[25]. Brooks *et al.* also carried out similar DFT calculations for a *ppy*Pt(acac) complex[26], the results were visualised as a contour plot of the HOMO and LUMO orbitals (Figure 14).

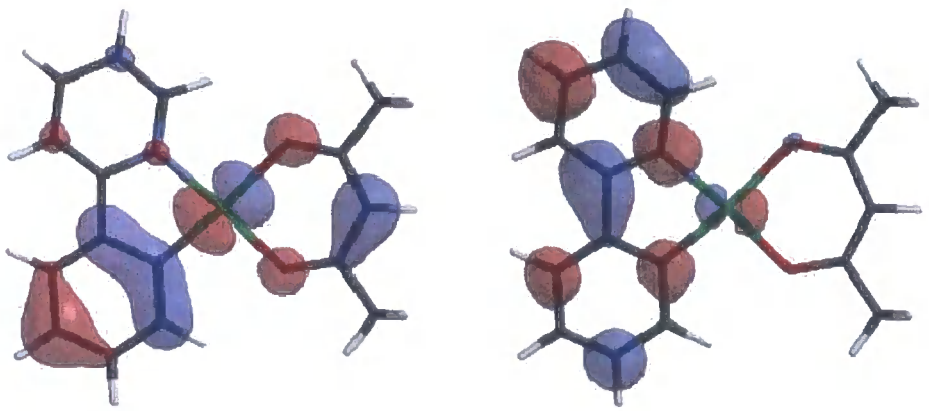

Figure 14 – Contour plots of the HOMO (left) and LUMO (right) orbitals in $Pt(ppy)_2(acac)$ from Brooks et al.. For clarity, only one ppy ligand is shown.

Figure 14 shows that the HOMO is a mixture of phenyl and platinum orbitals whereas the LUMO is predominantly located on the 2-phenylpyridine ligand. This plot has been shown as it is easier to visualise than the data for *fac*-$Ir(ppy)_3$ and the position of the HOMO and LUMO orbitals are very similar for both complexes.

Using the information in Figure 14 the shifts in λ_{max} emission in Table 1 can be explained. It can be seen that there is a large LUMO electron density at the 2- and 4-positions of the phenyl ring. There are two complexes with an F group on the 2- and 4-positions of the phenyl which brings about a shift in emission of the complex. The F group acts as a weak π-donor which raises the level of the LUMO; this increases the band gap and blue shifts the emission to λ_{max} = 514 and 506 nm for the 2-F and 4-F, respectively. There is a large HOMO electron density on the 3-position of the phenyl. When a CF_3 group is placed on the 3-position of the phenyl it acts as an electron withdrawing group and removes electron density from the HOMO, lowering the HOMO level, and increasing the band gap therefore blue shifting the emission to λ_{max}= 517 nm. Similarly when a CF_3 group is placed in the 5-position on the pyridine it interacts with the LUMO removing electron density and lowering the level which reduces the band gap and red shifts the emission to λ_{max}= 545 nm. When a strong electron donating group is placed on the phenyl such as a methoxy group in the 3-position (large HOMO electron density) we can see a large red shift in emission due to the increased HOMO level (λ_{max} = 595 nm).

Many different ligands have been cyclometalated onto Ir often as a derivative of the 2-phenylpyridine ligand forming both tris- and bis-cyclometalated complexes[27]. Lamansky *et al.* reported a number of variants of bis-cyclometalated iridium complexes and their use in OLEDs. The structures **11-25** synthesised by Lamansky *et al.* can be seen below. For clarity the (acac) ligand is not shown.

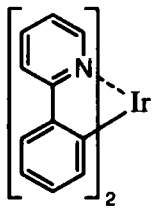

ppy (**11**)

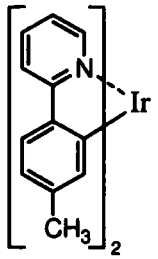

tpy (**12**)

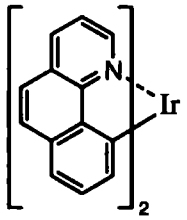

bzq (**13**)

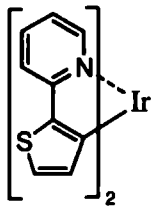

thp (**14**)

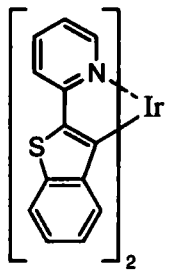

btp (**15**)

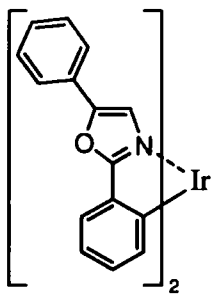

dpo (**16**)

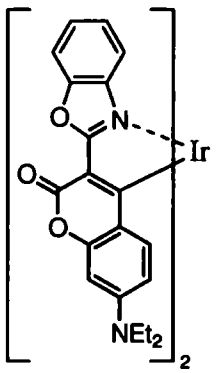

C6 (**17**)

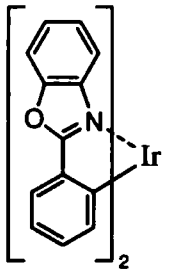

bo (**18**)

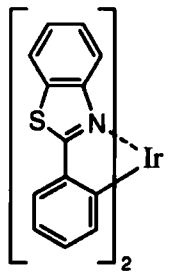

bt (**19**)

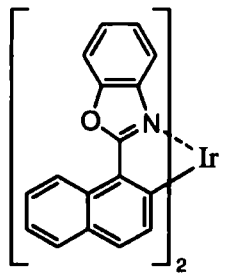

bon (**20**)

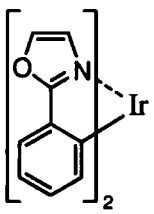

op (**21**)

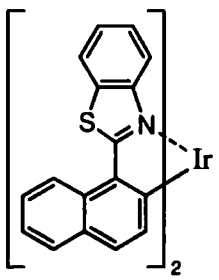

αbsn (**22**)

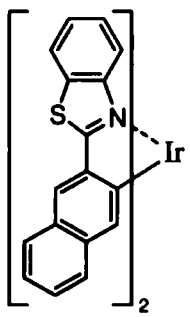

βbsn (**23**)

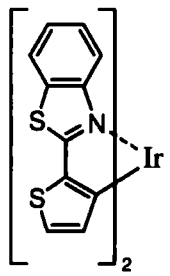

btth (**24**)

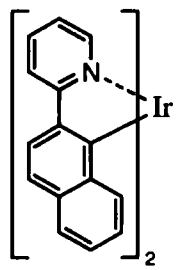

pq (**25**)

Emission in the complexes is thought to predominantly originate from the MLCT bands. The emission of the non-ppy or ppy derivative complexes with (acac) as the ancillary ligand varied from 520 nm (**21**) to 612 nm (**15**) with internal quantum efficiencies varying between 10% (**16** and **25**) and 60% (**17**). **17** is a common fluorescent laser dye which demonstrates no observable phosphorescence and

high quantum efficiency for fluorescence at room temperature. Strong ISC is demonstrated in **17** through the shift in the emission maxima when comparing the emission of just the C6 ligand to the emission of the complex (500 nm and 570 nm, respectively). The red shift demonstrates the strong ISC when excitons migrate from the ^{1}MLCT state to the ^{3}MLCT state.

Iridium complexes have also found a use in the search for white light from an OLED. These so called WOLEDs emit over a broad spectrum producing 'white' light (ideal CIE co-ordinates are 0.333, 0.333). There are several different methods used to produce white light from an OLED. A combination of emitters is a favoured method utilising red, green and blue emitters in the right concentrations can product white light[28]. The problem with this strategy is that excitons can be transferred from the blue to green emitters and the green to red emitters resulting in a red shifted emission if dopant concentrations are not precisely controlled. **26** was used as a dopant and exciton blocking layer in a WOLED device[29]. See structure below.

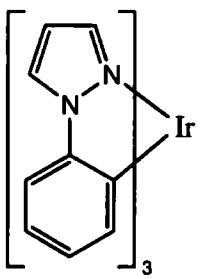

fac-Ir(ppz)$_3$ (**26**)

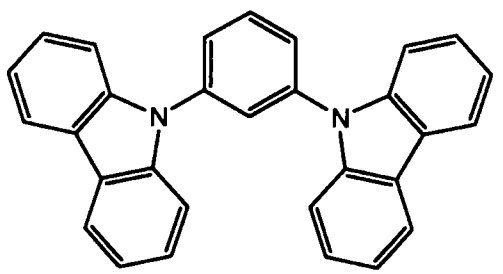

mCP (**27**)

In a previous effort to produce white light using a single dopant and an ITO/NPD/CBP (**9**):dopant/BCP (**10**)/Alq$_3$ (**3**)/LiF/Al device structure[30] there was exciton leakage into the NPD HTL layer leading to NPD emission and a blue shift of the emission moving away from white light. A dopant was needed that could act as an exciton blocker within the CBP layer ensuring excitons could not reach the NPD layer to emit. Ir(ppz)$_3$ meets all the criteria for an efficient exciton blocker, such as a high LUMO level to block electrons and a HOMO level above that of the HTL. The device produced nearly white light at a peak brightness of 8000 cd/m^2 with a maximum quantum efficiency of 3.3%. Use of a mCP (**27**) host and higher dopant concentrations increased the quantum efficiency to a maximum of 6.4%, the highest seen from a WOLED at the time.

Work in our group established that efficient two-component WOLEDs could be fabricated using a single active layer containing blue-emitting polyfluorene host and a yellow-orange-emitting iridium tris(tri-fluorenyl)pyridine guest. The two emitted colours complement each other and doping levels of 2–3% produced stabilised emission with CIE coordinates 0.348, 0.367 close to pure white. A peak

external quantum efficiency of 2.8%, and luminance of 16000 cd/m^2 at applied voltage of 5 V (*i.e.*, 4.57 cd/A) was obtained[31].

1.4.3 *Facial* and *Meridional* Tris-cyclometalated Ir Complexes

In tris-cyclometalated complexes an important factor that must be considered is the configuration of the ligands around the Ir centre, *i.e.* a *facial* (*fac-*) or *meridional* (*mer-*) complex. The difference between *fac-* or *mer-* complexes can be seen in Figure 15.

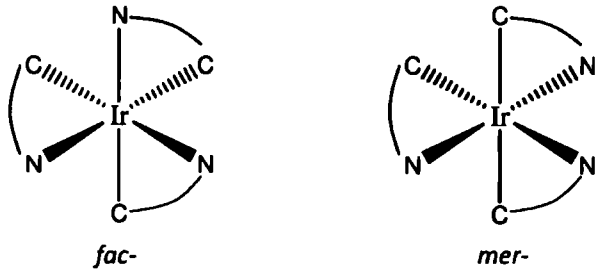

Figure 15 – Schematic of facial and meridional isomers

This different ligand configuration gives rise to a difference in optical properties of the two isomers. In 2003 a study was under taken by Tamayo *et al.* into the difference between several facial and meridional iridium complexes with interesting results[32]. The complexes synthesised are shown below.

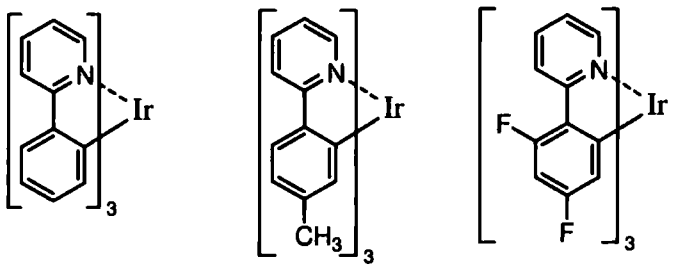

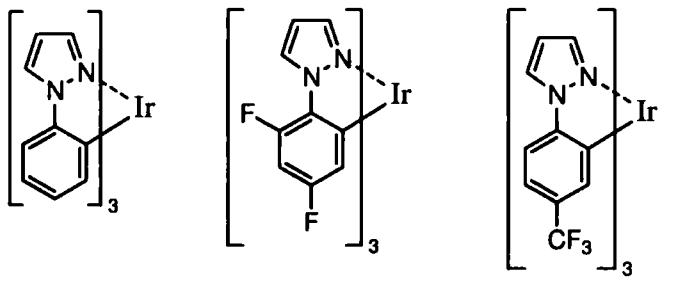

It was found that *mer-* complexes were red shifted over their *fac-* counterparts, with an emission maximum shift of 38 nm for tpy. The *mer-* complexes give poor quantum photoluminescence efficiencies relative to the *fac-* isomers by *ca.* an order of magnitude. From these results it became clear that *mer-* complexes are not suited to OLED applications. The paper raised a number of interesting observations. The *mer-* complex is thought to be the kinetic product of a reaction to produce a tris-cyclometalated iridium complex whilst the *fac-* isomer is the thermodynamic product. The *mer-* complex can be synthesised by reaction at a lower temperature for a shorter time, whereas the *fac-* complex required higher temperature and longer reaction time. *Mer-* complexes can be converted to their *fac-* counterparts by heating in a high boiling point solvent such as glycerol or irradiating the complex with a UV lamp in a co-ordinating solvent such as DMSO. The two isomers are readily identifiable by ^{1}H NMR spectra as the *fac-* complexes exhibit much simpler spectra due to equivalence of all the protons on the same position on each ligand.

1.4.4 Carbazole and Ir Complexes

As the work later in this thesis will focus on carbazole forming the basis of cyclometalating ligands for Ir an overview of the previous work on this subject will now be given.

Carbazole (**32**) is an electron rich aromatic system, that is highly conjugated which makes it an excellent candidate for OLED work and in combination with a pyridyl substituent forms a ligand which can cyclometalate in a similar fashion to 2-phenylpyridine. Very few examples exist in the literature of a carbazolyl moiety directly cyclometalated to a metal centre such as Ir. The few examples that do exist are described below.

The first cyclometalation directly onto a carbazole unit - specifically (pyridin-2-yl)carbazole was reported in the Bryce group in 2005[33] who synthesised the two parent ligands **33** and **34**.

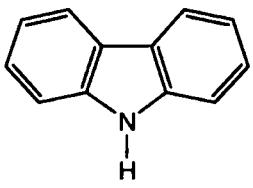

Carbazole (**32**)

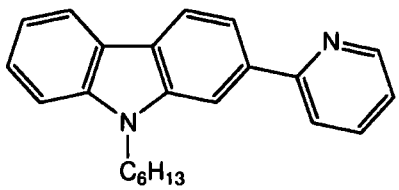

(Pyridin-2-yl)carbazole (**33**)

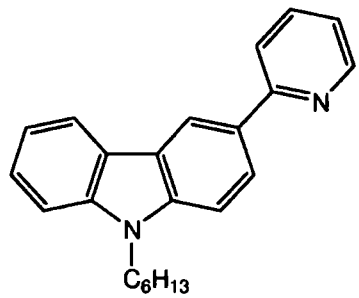

(Pyridin-3-yl)carbazole (**34**)

By analogy with 9,9-dialkylfluorene units the carbazole nitrogen has an alkyl group attached for added solubility. This also aids the solution processability of the derived Ir complex when forming layers for an OLED device by spin-casting from solution. The variants of the parent complexes shown above included fluorene groups (one or two) in-between the pyridyl and the carbazole units. Photophysical studies on the complexes[34] demonstrated a 90 nm shift between the pyridin-2-yl [Ir(Cz-2-Py)$_3$] and the pyridin-3-yl [Ir(Cz-3-Py)$_3$] carbazole iridium complexes. The [Ir(Cz-2-Py)$_3$] complex gave an emission maximum of 500 nm whereas the [Ir(Cz-3-Py)$_3$] complex was at 590 nm. This can be attributed to the position of the N in the carbazole system. In the [Ir(Cz-2-Py)$_3$] system the N is *para-* to the Ir centre with strong electron donation to the Ir, raising the HOMO level and lowering the band gap hence red shifting the emission of the complex. The emitting state of the complexes are thought to be a mixture of MLCT and π-π^* states. External EL quantum efficiencies of 1.3% and 0.06% were achieved for the [Ir(Cz-2-Py)$_3$] and [Ir(Cz-3-Py)$_3$] complexes, respectively, as blends in a polyfluorene-based host, in a simple solution processed device, with no additional HT or ET layers. The quantum efficiency of the [Ir(Cz-2-Py)$_3$] complex is higher due to an increased exciton trapping efficiency compared to the [Ir(Cz-3-Py)$_3$] complex. It was concluded that a host with a higher triplet energy is needed to fully exploit these complexes as dopants as the host used has a low lying triplet energy leading to quenching of the triplet excitons on the complexes. The complexes showed quantum photoluminescence efficiencies of 28% and 39% for [Ir(Cz-2-Py)$_3$] and [Ir(Cz-3-Py)$_3$], respectively.

In 2006 Wong *et al.* published very similar Ir complexes[35] to those previously reported in our group, with *N*-phenyl substituents, see below.

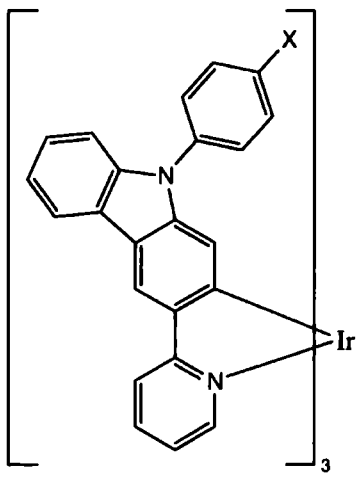

fac-[Ir(x-Cz-py)$_3$]
X = H (**35**), F (**36**)

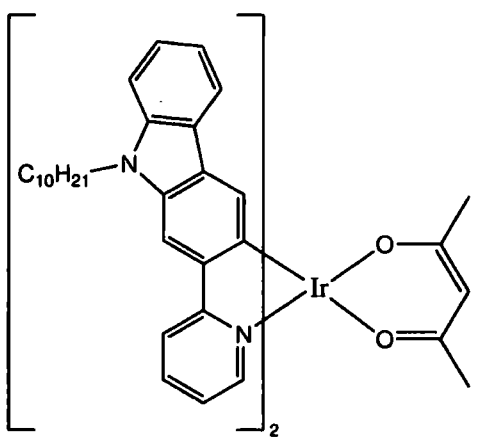

Ir(2-PyDeCz)$_2$(acac) (**37**)

The complexes **35** and **36** show very similar solution emission spectra with maxima of 515 nm and 514 nm, respectively. This is explained by the lack of HOMO or LUMO electron density on the *N*-phenyl ring, as from the reported DFT calculations; hence the substituent group has little effect on the emission spectrum of the complexes. The reported multilayer device structure of ITO/NPB/CBP(**9**):complex/BCP(**10**)/Alq_3(**3**)/Mg:Ag was fabricated by thermal evaporation techniques requiring a large amount of the complex to be synthesised, *ca.* 100 mg per device. The BCP layer aids the confining of excitons within the CBP host layer as it blocks the passage of excitons to the Alq_3 ET layer. The device using complex **35** demonstrated a very high external quantum efficiency of 11.6% which was explained by the charge balancing features of the carbazolyl moiety.

A bis-cyclometalated example of a carbazole directly bonded to an iridium centre (**37**) was published in 2008 by Tao *et al.*[36] (*vide supra*). This complex showed a photoluminescence emission maximum at 594 nm attributed to the MLCT state. In a device (standard configuration - ITO/PEDOT:PSS/CzOXD:**37**/BCP(**10**)/Alq_3(**3**)/LiF/Al) the emission maximum was *ca.* 613 nm, changing slightly with device configuration and dopant concentrations.

1.5 Conclusion

OLEDs have progressed at a rapid rate and can be expected to do so for the foreseeable future. Fluorescent emitters were usurped by phosphorescent guests and hosts and the goal of 100% internal quantum efficiency has effectively been realised with some phosphors. External quantum efficiencies and hence power consumption efficiencies as well as device fabrication expertise are improving to the point that an OLED TV has been commercialised in early 2008. Iridium complexes form the forefront of phosphorescent guests and can be expected to lead the small molecule OLED sector. Cyclometalated ligands based on 2-phenylpyridine make excellent OLED candidates when combined with an Ir centre. It has recently been established that carbazole can be directly cyclometalated onto Ir opening up another avenue to explore and exploit. This will form the basis of the work described in the remainder of this thesis.

Chapter 2 – Novel Functionalised Iridium Complexes

The aim of this chapter is to introduce the reader to the new iridium (III) complexes synthesised in the progression of this work. This chapter will also discuss the methodology of the syntheses used as well as the results from other investigations into the properties of the complexes such as their photophysical properties.

2.1 Synthesis

As shown in Chapter 1.4 iridium complexes comprise a generation of electrophosphorescent guests in OLED devices and excel in their performance. Functionalisation of the ligands in these complexes can lead to significant shifts in absorbance and emission spectra. With a possible end use of these complexes in mind as components in information displays, the ability to tune a 'parent' complex's electroluminescent spectrum is a great aid. For example, if several structurally different complexes had to be synthesised for the RGB components of a display this would be more costly than simply functionalising one parent complex.

Aside from advantages to companies involved in the fabrication of products using OLED technology, understanding exactly how functionalisation affects the optical properties of these complexes is of fundamental interest and will continue to have an effect on the design of these complexes.

2.1.1 Parent Complexes

The parent complexes involved in this work were originally published by our research group in 2005[33, 34]. This work follows on from the work undertaken into cyclometalation of carbazole onto an iridium (III) centre as described in Chapter 1.4.4. The complexes synthesised were the first examples of the direct cyclometalation of carbazole onto iridium. Complexes **38** and **39** are the parent complexes which form the basis of the new work presented here.

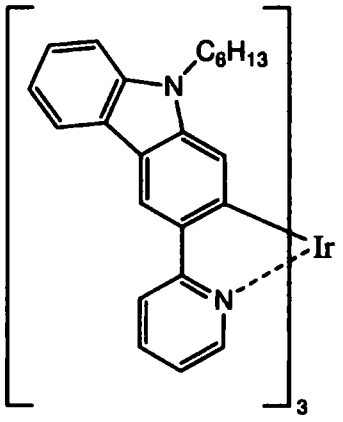

38

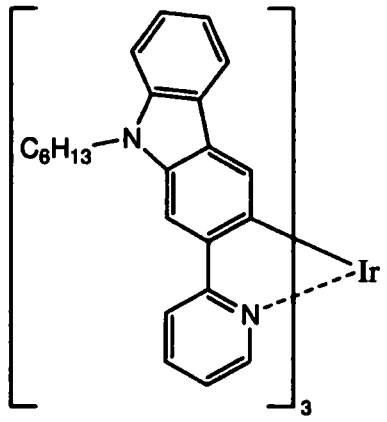

39

To affect the photophysical properties of the complexes the HOMO and LUMO levels must be changed. To do this electron withdrawing groups (EWGs) or electron donating groups (EDGs) can be added to the ligands. The ligands presented in these parent complexes are analogous to 2-phenylpyridine ligands, with carbazole replacing the phenyl. In order to determine where the functionalisation would have the largest effect the position of the HOMO and LUMO DFT calculations from Hay[25] were consulted. Hay's calculations show a high LUMO density on the pyridine and a high HOMO density on the phenyl. It was decided that for the largest effect the 4- and 5-positions on the pyridine ring would be functionalised in separate complexes with an EWG and an EDG.

A trifluoromethyl (CF_3) group was chosen as the EWG for the electronegativity effect of this group in removing electron density from the aromatic system. The CF_3 group was chosen over a fluoro (F) group as halogens exhibit a mixed electron donating and electron withdrawing effect on aromatic systems through π-donation and electronegativity respectively. A methoxy (OMe) group was chosen as the EDG as it has a strong electron donating effect on aromatic systems increasing the electron density.

This gives a series of eight iridium (III) complexes (**40 – 47**) as the initial target complexes in this work (*vide infra*).

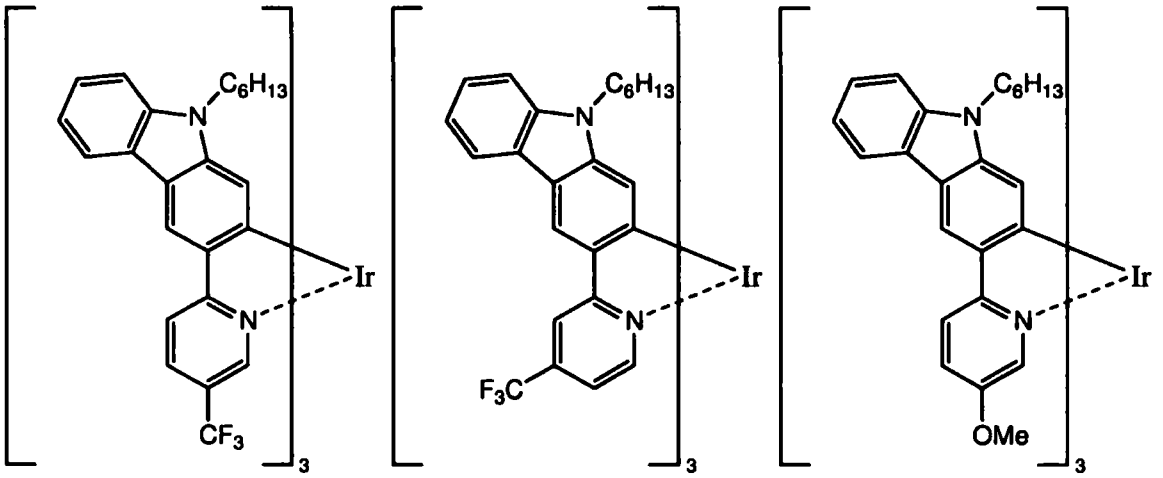

40 **41** **42**

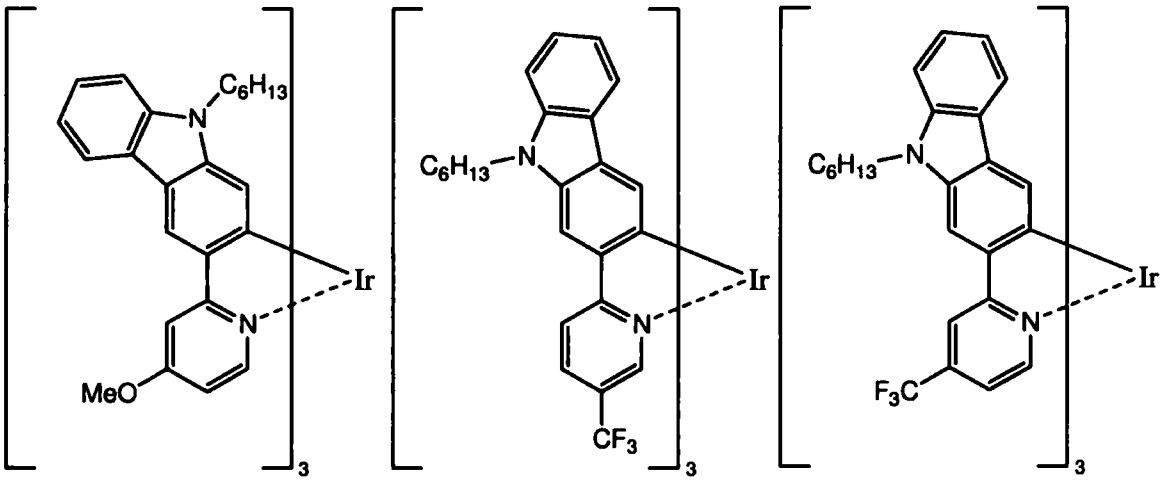

43 **44** **45**

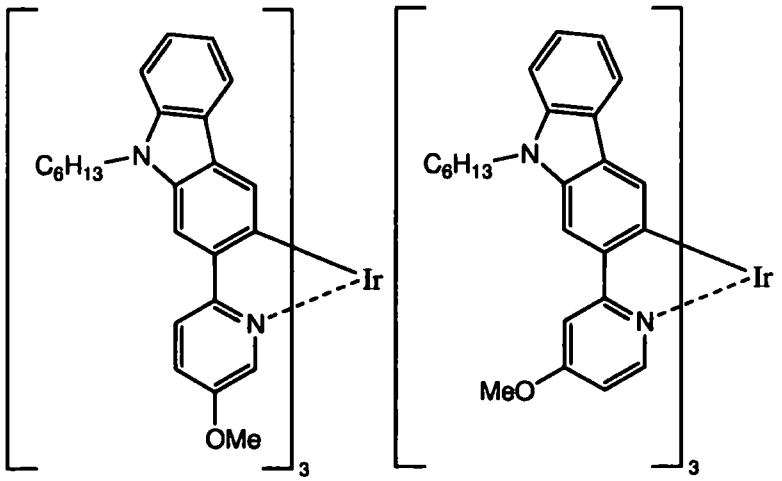

46 **47**

These constitute two series of complexes, distinguished by the position of the functionalised pyridyl in relation to the carbazolyl moiety. In series 1 (complexes **40** to **43**) the pyridyl is attached to the 3-position of carbazole; in series 2 (complexes **44** to **47**) the pyridyl is at the 2-position of carbazole.

The general synthetic route to the complexes was based on the original route to the parent complexes[33, 34] from either 2-bromocarbazole (**48**) or 3-bromocarbazole (**49**) as starting materials to **38** and **39**.

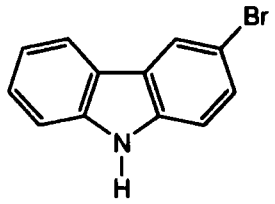

48

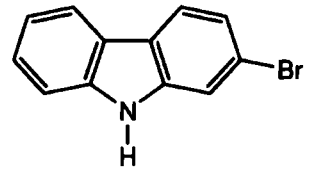

49

2.1.2 Synthetic Route to the Starting Materials

Selectively forming a singly brominated carbazole is an interesting synthetic problem. This is due to the directing nature of the secondary amine group. Although the lone pair of the N is more involved in the aromatic structure than a standard secondary amine it still directs bromination primarily to the *ortho* and *para* positions. For the synthesis of 3-bromocarbazole this problem was alleviated by control of the equivalents of brominating agent or bromine in the bromination reaction. It was found by Tavasli *et al.* that 1.1 equivalents of bromine in DMF at 0-20 °C over 1-27 h produced a yield of 35% of 3-bromocarbazole from carbazole with 3,6-dibromocarbazole **50** as the byproduct (2% yield).

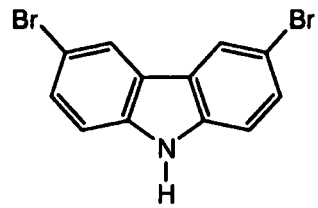

50

Producing 2-bromocarbazole is, relatively, more complex. The amine group does not activate the *meta* position on carbazole for bromination, therefore, carbazole cannot be used as a starting material. Tavasli *et al.* produced 2-bromocarbazole starting from 2,5-dibromonitrobenzene (**51**). This underwent a Suzuki coupling reaction with phenylboronic acid (**52**) (1.0 equivalents) to form 2-nitro-4-bromo-biphenyl (**53**) as can be seen in Reaction Scheme 1 (*vide infra*). An expected by-product of this reaction is the formation of compound **54**.

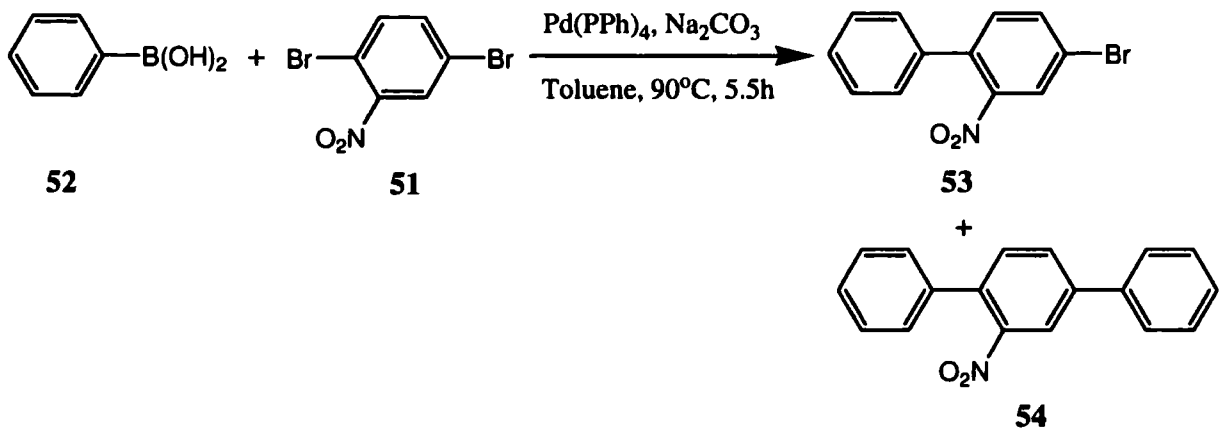

52 51 53 + 54

Reaction Scheme 1 – Formation of 2-nitro-4-bromobiphenyl

If the reaction was not optimised for the synthesis of the target compound **53**, then a larger amount of **54** would be produced making this route unviable for producing 2-bromocarbazole. The separation of **53** and **54** was difficult, but as the by-product will not be able to react in a Suzuki reaction to form the ligand it was deemed that the separation was also unnecessary.

The next step of the route is to cyclise **53** to 2-bromocarbazole. This is done via a reaction with triethylphosphite, $P(OEt)_3$, which also acts as a solvent in the reaction. The products isolated are 2-bromocarbazole (**49**) and 2-phenylcarbazole (**55**, produced from the cyclisation of **54**).

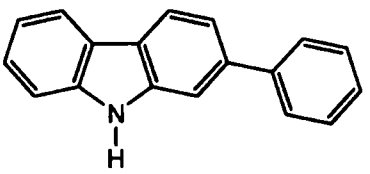

55

This route gave an overall yield 38% of 2-bromocarbazole (**49**) relative to the starting materials **51** and **52**.

Other routes were investigated in the progression of this work in an attempt to simplify the synthesis and improve on the yield.

The first route was an attempted one-step ring closure reaction of **56** (commercially available) to 2-bromocarbazole via the reaction with a palladium acetate or similar (see Reaction Scheme 2).

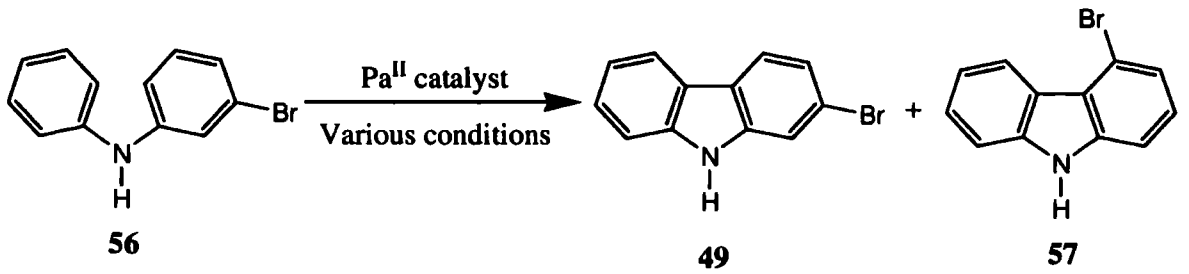

56 49 57

*Reaction Scheme 2 – One step formation of 2-bromocarbazole; **49** could not be purified from the multi-component product mixture*

This reaction was following a recent report of the synthesis of a substituted carbazole compound[37] using palladium acetate in a catalytic amount (10 mol%) and copper acetate (2.5 equiv.) to reform the palladium (II) species. The reaction was high yielding at 72%. This reaction is originally based on work published in 1975[38] on these types of ring closing reactions forming substituted carbazole compounds or similar aromatic heterocyclic compounds. The earlier work used palladium acetate in equivalent amounts and did not utilise copper acetate to reform the catalytic species, hence lower yields were reported. It should be noted that neither of the published works mentioned attempts to produce a carbazole compound substituted at the 2-position.

The initial attempt to produce 2-bromocarbazole from **56** utilised the same reagents as in the 2006 paper, namely palladium acetate (10 mol%) and copper acetate (2.5 equiv.). However, the desired product was not identified in the multi-component product. A change of catalyst to palladium trifluoroacetate (1.0 equiv.) produced 2-bromocarbazole **49** (^{1}H NMR and MS evidence).

However, ^{1}H NMR analysis established that 64% of the product mixture was 2-bromocarbazole, the remainder being 4-bromocarbazole **57** (formed by ring closure *ortho* to the bromine substituent) and unreacted starting material. The yield of 2-bromocarbazole was 36%, comparable to the original route to this compound by Tavasli *et al.*. The use of palladium trifluoroacetate in an equivalent fashion makes the reaction very expensive; this, combined with the inseparable product mixture led to the conclusion that this was not a viable alternative route for the synthesis of 2-bromocarbazole.

The second route investigated was similar to the synthesis used by Tavasli *et al.* in that it relies on the cyclisation of a nitro-biphenyl compound. This route was designed to eliminate the possibility of forming by-products such as **54** and **55**. The route involves the bromination of 2-nitrobiphenyl (**58**) to 4-bromo-2'-nitrobiphenyl (**59**) followed by cyclisation to 2-bromocarbazole (Reaction Scheme 3).

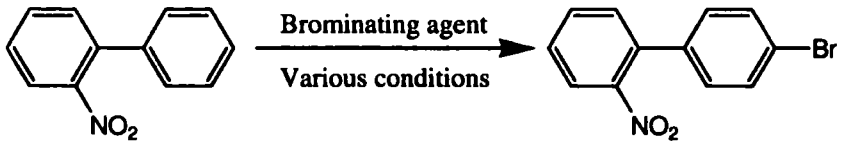

58 **59**

*Reaction Scheme 3 – Bromination of 2-nitrobiphenyl to 4-bromo-2'nitrobiphenyl; **59** could not be purified from the multi-component product mixture*

It was thought that the 2-nitro group would deactivate the benzene ring to bromination leaving the most activated site as the proposed 4'-position. The reaction was attempted several times using several variables such as the use of bromine and N-bromosuccinimide (NBS) as brominating agents; chloroform, acetic acid and water were used as solvents; the temperature and time of the reactions were also varied. After the working up of these reactions it was determined from thin-layer chromatography that the separation of the starting material and product **59** (for which there was ^{1}H NMR evidence) was not possible and the route was not explored further.

After exploring these separate routes to produce 2-bromocarbazole it was decided that the most efficient and reliable route was the original procedure of Tavasli *et al.*[33].

2.1.3 Synthetic Route from Starting Materials to Complexes

The formation of the complexes starting from 2- and 3-bromocarbazole is a relatively simple process. The starting materials (**48** and **49**) were N-alkylated for added solubility and ease of handling, which also aides the solubility of the final complexes.

The boronic acid species, **60** and **61**, were formed from the starting materials, **48** and **49**, as shown in Reaction Scheme 4.

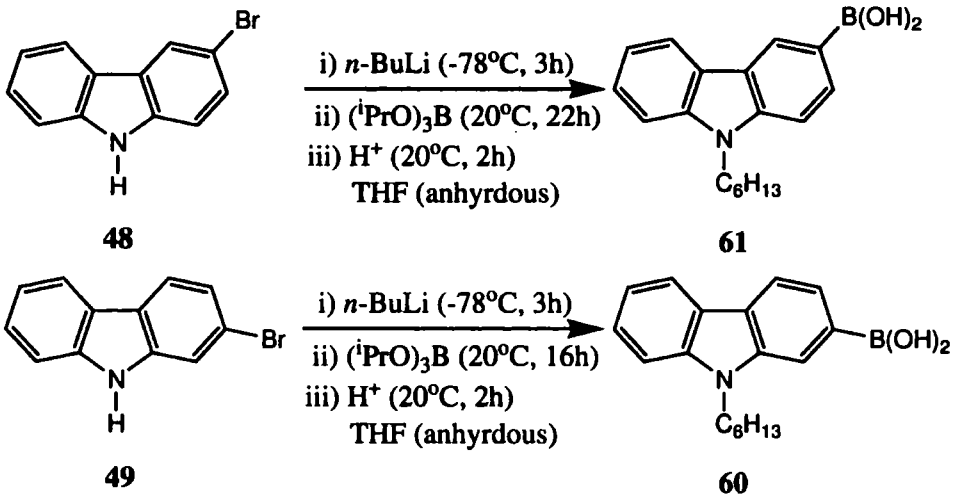

*Reaction Scheme 4 – The formation of the boronic acid species, **60** and **61**, from the starting materials, **48** and **49**).*

The ligands are formed through a Suzuki reaction with the appropriate boronic acid (**60** or **61**) and the functionalised halopyridine partner. Two catalysts were used separately in the Suzuki reactions, namely bis(triphenylphosphine)palladium(II) dichloride and tetrakis(triphenylphosphine)palladium(0).

The synthesis of the Ir complexes was originally performed in our group by Tavasli *et al.* with the use of a microwave reactor, although in the present work the reactions were performed at high temperature in glycerol using $Ir(acac)_3$ to form the thermodynamically favoured *facial* isomers[32] (Reaction Scheme 5)

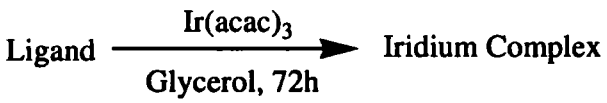

Reaction Scheme 5 – General scheme for the formation of Ir complexes

The synthesis of complexes **46** and **47** (involving ligands where the OMe group is *para* to the N on the pyridyl) did not proceed as expected. The reactions were carried out in the same manner as all other reactions performed to synthesise the complexes. Analysis of the reactions by thin-layer chromatography showed that many compounds were present in the reaction mixture and subsequent separation by column chromatography on silica could not isolate the complexes. The reason for the failure of these reactions is thought to be linked to the bonding of the N on the pyridine to the iridium centre and the fact that there is an electron donating methoxy group *para* to this position.

As an interesting observation it is noted that there is the potential for a regioisomer of the complexes to be formed if cyclometalation occurred at the alternative carbon atom (**41a**).

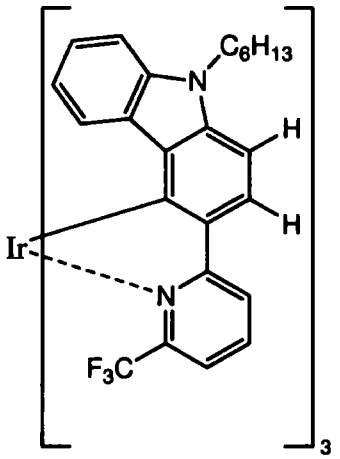

41a

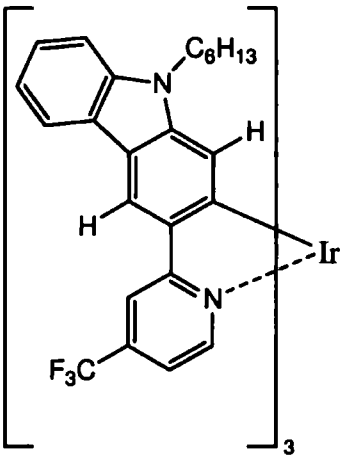

41

However, this regioisomer was not observed in any of the complexes probably through steric hindrance of the ligands around the Ir centre. In the complexes shown above two protons have been indicated which aid in distinguishing the complexes from one another. In complex **41** ^{1}H NMR would show the two protons as singlets whereas in complex **41a** the two protons would be doublets. As can be seen in Chapter 3 complex **41a** is not formed as the complexes clearly demonstrate three distinct singlets from the two protons shown above in complex **41** and the proton in the 3-position on the pyridyl. The three singlets are indicated on the example ^{1}H NMR spectrum of complex **41** shown in Figure 1.

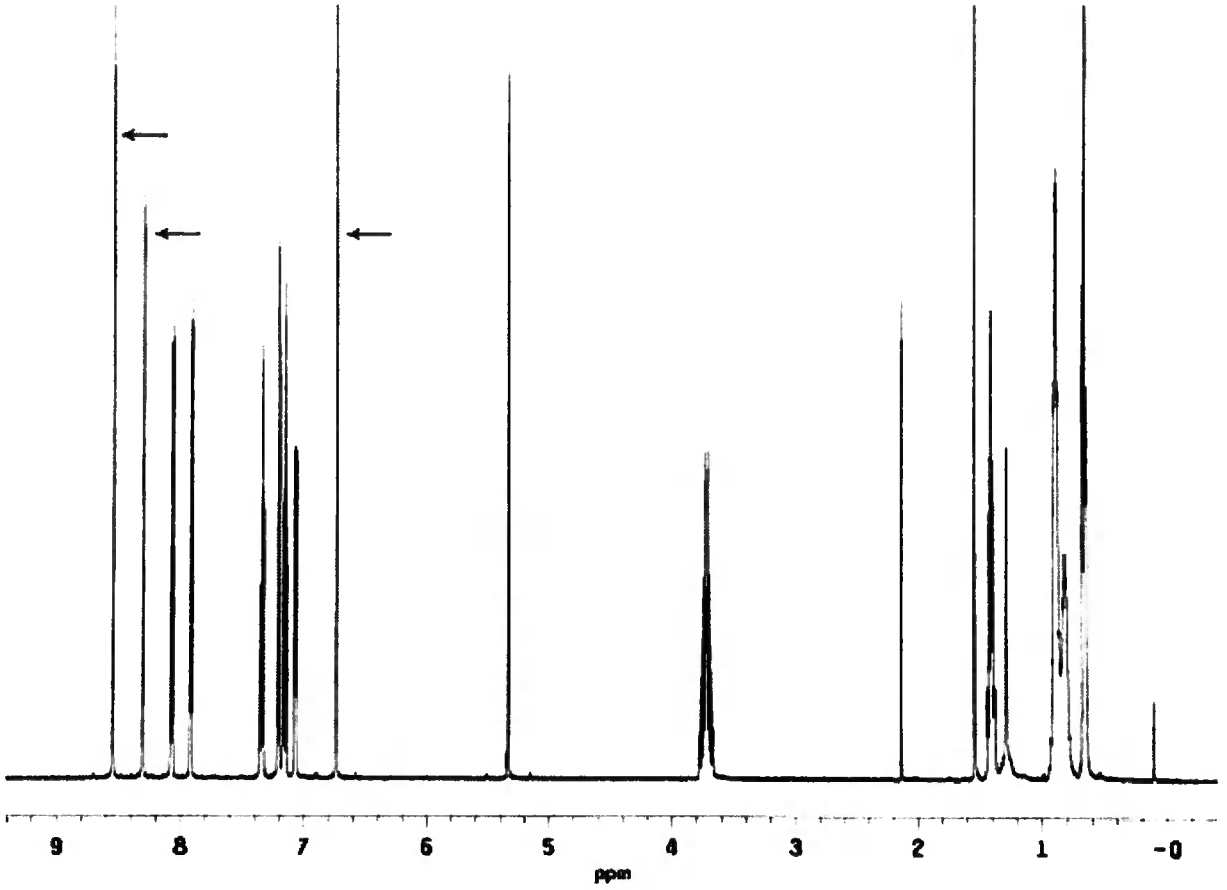

Figure 1 – ^1H NMR of complex 41 in CD_2Cl_2

2.2 DSC/TGA Investigation

Investigations were carried out into the thermal characteristics of the complexes using differential scanning calorimetry (DSC) and thermal gravimetric analysis (TGA) techniques.

DSC studies were performed for complexes **40**, **41** and **42**, *i.e.* the series in which the pyridyl on the carbazole is in the 3-position. Analysis of the available DSC data showed that the complexes are amorphous solids which do not undergo any transitions between 0 to 300 °C. There is no evidence of crystallisation which was present in some of the complexes synthesised by Tavasli *et al.*. The complexes exhibit sharp melting points between 328 °C and 355 °C. It is predicted that complexes **43** - **47** would exhibit the same characteristics. Two peaks were observed for complex **40**, the first of which is thought to correspond to the boiling point of glycerol as a contaminant in the sample. Glycerol was the solvent used in the preparation of the complexes from the ligands and $Ir(acac)_3$. The second peak is thought to be the melting point of the complex at a similar value to those found for complexes **41** and **42**. A summary of the DSC data can be seen in Table 1 (*vide infra*).

TGA studies were performed for complexes **40, 41, 42, 45** and **46**. With the exception of **40** the temperature at which 5% weight loss occurred was over 350 °C and comparable with that of $Ir(ppy)_3$ at 413 °C[39]. The low value of $\Delta T_{5\%}$ for complex **40** is thought to be due to contamination of the sample with glycerol, the evaporation of this contaminant leads to the lowering of the expected $\Delta T_{5\%}$ value. With the exception of complex **40** the values all indicate that the complexes are stable up to relatively high temperatures of >350 °C. A summary of the TGA data can be seen in Table 1 below.

Complex	DSC Melting Point [°C]	TGA $\Delta T_{5\%}$ [°C]
40 $[Ir(Cz\text{-}3\text{-}Py(5\text{-}CF_3))_3]$	280, 333 (sharp)	231
41 $[Ir(Cz\text{-}3\text{-}Py(4\text{-}CF_3))_3]$	328 (sharp)	383
42 $[Ir(Cz\text{-}3\text{-}Py(5\text{-}OMe))_3]$	355 (sharp)	369
45 $[Ir(Cz\text{-}2\text{-}Py(4\text{-}CF_3))_3]$	-	387
46 $[Ir(Cz\text{-}2\text{-}Py(5\text{-}OMe))_3]$	-	358

Table 1 – Summary of DSC and TGA data

2.3 Cyclic Voltammetry Investigation

Cyclic voltammetric (CV) investigations were carried out at 298K using an $Ag/AgNO_3$ reference electrode and the ferrocene/ferrocenium couple[40] as a secondary reference. The supporting electrolyte was a 0.1M solution in DCM of tetra(*n*-butyl)ammonium hexafluorophosphate (nBu_4NPF_6). A scanning rate of 100 mV/s was used.

All complexes exhibited cleanly reversible oxidation potentials assigned to the Ir^{III}/Ir^{IV} couple. For comparative purposes the oxidation potentials of the parent complexes were also measured. A summary of the half-wave oxidation potentials can be seen in Table 2 (*vide infra*).

There is an appreciable difference of the oxidation potentials between the two series. On comparison of the complexes in series 1 to their counterparts in series 2 it is clear that the former are harder to oxidise. For example, when comparing **40** to **44** there is a shift of the oxidation potential to lower potentials (+ 0.752 V vs. + 0.541 V). In series 2 the N of the carbazolyl moiety is *para* to the Ir metal centre and thus its electron donating effect through the aromatic ring which destabilises the ground state of the complex, raising the HOMO level giving rise to lower oxidation values.

A difference in oxidation potentials is also noticeable between electron donating groups and electron withdrawing groups. This is comparable to the work discussed in Chapter 1.4.2 where Grushin *et al.*[24] functionalised phenylpyridine ligands on $[Ir(ppy)_3]$ (**8**). In the case of complexes **40** to **46** the functionalised unit is the pyridyl. If the level of the HOMO in the complexes is considered, the effect of an EDG or EWG has upon the oxidation potentials become apparent. An electron withdrawing group (such as the CF_3 group in complex **40**) removes electron density from the HOMO thus lowering its level and accordingly increasing the oxidation potential compared to the parent complex (+ 0.752 V vs. + 0.536 V, respectively). An electron donating group (such as the OMe group in complex **42**) increases electron density in the HOMO thus raising its level and decreasing the oxidation potential compared to the parent complex (+ 0.486 V vs. 0.536 V, respectively). The increased oxidation potential is observed for all complexes where an EWG is present (**40**, **41**, **44**, **45**) and *vice versa* for complexes **42** and **46**.

The ligand centered oxidations in the complexes are observed as two and three-electron waves. They have higher potentials relative to the Ir^{III}/Ir^{IV} couple, an example of which can be seen in the cyclic voltammogram shown in Figure 2. The processes are quasi-reversible unlike the fully reversible Ir^{III}/Ir^{IV} couple that can be seen at the lower oxidation values.

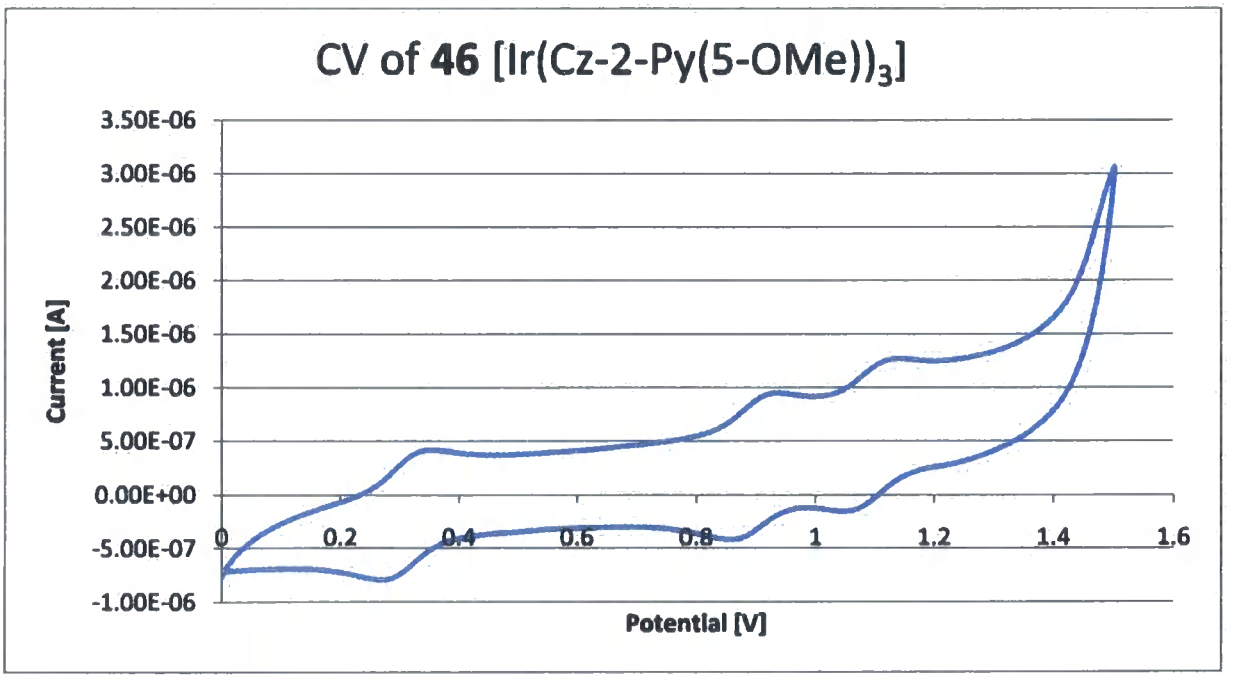

Figure 2 – Cyclic Voltammogram of **46** *$[Ir(Cz\text{-}2\text{-}Py(5\text{-}OMe))_3]$, averaged values over three scans show (***46** *vs. $Ag/AgNO_3$ in CH_2Cl_2), see Table 2.*

2.4 Photophysical Investigation

Solution state photophysical properties were ascertained using freshly prepared solutions of the complexes **40**, **41**, **42**, **44**, **45** and **46** and their parent complexes, **38** and **39**, in toluene. Emission measurements were taken using solutions which were degassed thoroughly using the repeated freeze-thaw technique. All measurements were taken using 1cm pathlength quartz cuvettes. Series 1 absorption measurements were taken using a Unicam UV/Vis Spectrometer UV2. Series 2 absorption measurements were taken using a Perkin Elmer UV/Vis Spectrometer Lambda12. All emission measurements were taken using a Jobin-Yvon Horiba Spex Fluorolog Spectrometer. A summary of the absorption and emission data can be seen in Table 2.

Complex	Absorption λ maxima [nm]	Emission λ maxima [nm]	$E^{ox}_{1/2}$ [V]
38 Series 1 parent [Ir(Cz-3-Py)$_3$]	329	504	+ 0.536
40 [Ir(Cz-3-Py(5-CF_3))$_3$]	326	536	+ 0.752
41 [Ir(Cz-3-Py(4-CF_3))$_3$]	323	558	+ 0.753
42 [Ir(Cz-3-Py(5-OMe))$_3$]	313	514	+ 0.486
39 Series 2 parent [Ir(Cz-2-Py)$_3$]	334	589	+ 0.480
44 [Ir(Cz-2-Py(5-CF_3))$_3$]	350	633	+ 0.541
45 [Ir(Cz-2-Py(4-CF_3))$_3$]	369	637	+ 0.532
46 [Ir(Cz-2-Py(5-OMe))$_3$]	346	577	+ 0.312

Table 2 – A summary of CV half-wave potentials and absorption and emission λ maxima

2.4.1 Absorption

The absorption spectra of the complexes in series 1 can be seen in Figure 4, the absorption spectra of the complexes in series 2 can be seen in Figure 5 (*vide infra*). *N.B.* For clarity the two series were not combined onto one figure.

The complexes exhibit the strongest absorbance bands between approximately 300 to 350 nm for series 1, and 325 to 375 nm for series 2. It is observed that the functionalised complexes exhibit very similar absorption spectra to their parent complexes and in analogy to the original photophysical investigation of the parent complexes[34] these bands are assigned as $^1\pi$-π^* transitions. The weaker absorptions at *ca.* 375 nm for series 1 and 450 nm for series 2 are assigned to ^{1}MLCT transitions. Very weak absorptions assigned to ^{3}MLCT transitions can be observed at longer

wavelengths. These assignments are made by analogy with previously reported iridium complexes[24, 34, 41] of a similar structure and TD-DFT calculations performed (*vide infra*). As an example the absorption spectrum of complex **42** is shown in Figure 3 with the absorption peaks assigned to specific transitions.

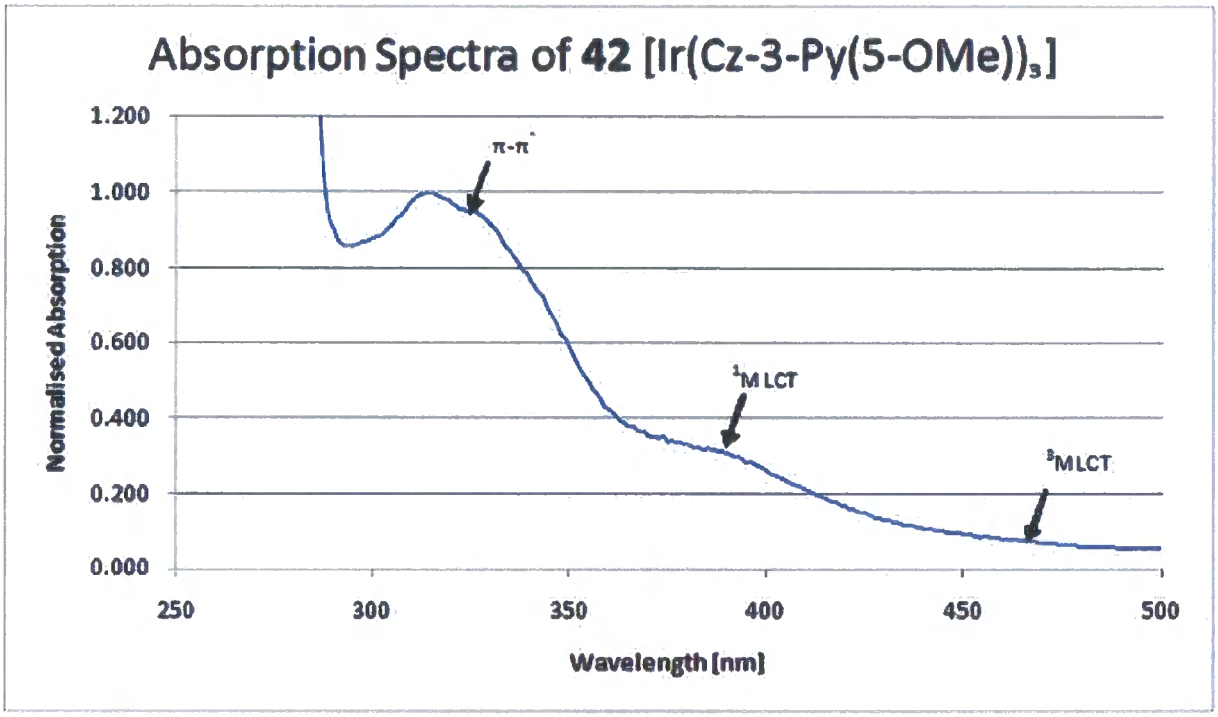

*Figure 3 – Assigned bands in the absorption spectra of complex **42** [Ir(Cz-3-Py(5-OMe))$_3$] in degassed toluene solution at 298 K*

Upon comparison of the absorption spectra and maxima observable from Table 2 and Figures 4 and 5 it is clear that series 2 exhibits red shifted absorbance spectra relative to series 1. This can be compared with the CV results reported in Chapter 2.3 (*vide supra*). Series 1 exhibited higher oxidation potentials than series 2. This is due to the position of the N in the carbazolyl moiety in the two series. In series 2 the N is *para* to the Ir metal centre, and has a large electron donating effect which destabilises the HOMO thus raising the level and lowering the gap between HOMO and LUMO. A smaller band gap means lower energy light will be absorbed thus red shifting the absorption relative to series 1 where there is not such a strong electron donating effect from the *meta* N.

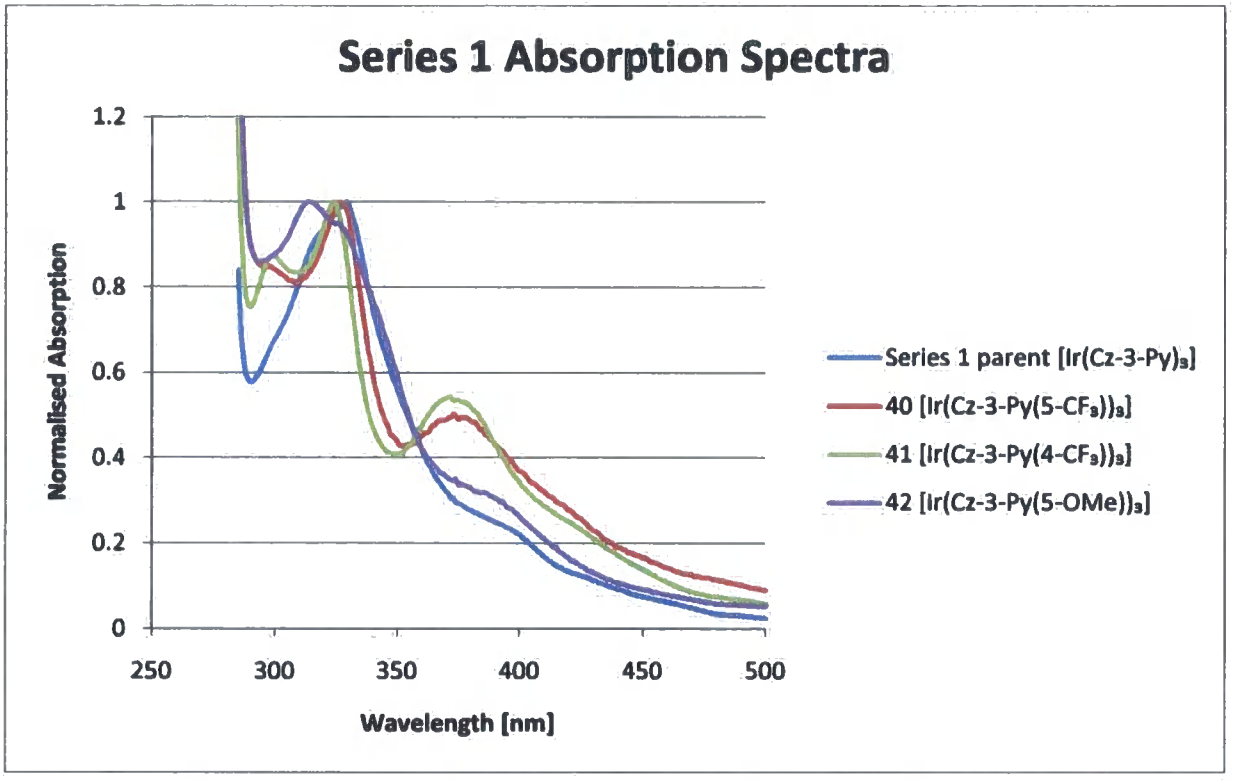

Figure 4 – Normalised absorption spectra of series 1 complexes and their parent complex in degassed toluene at 298 K

From Figure 4 it can be seen that the ^{1}MLCT absorbance has increased for complexes **40** and **41** when an EWG (CF_3) is present. Interestingly, all complexes are blue shifted relative to the parent complex. The EDGs and EWG are all attached to the pyridyl moiety of the complex which exhibits a large amount of LUMO density and a very small amount of HOMO density. Therefore, the groups must be effecting the position of the LUMO. An EWG would be expected to lower the level of the LUMO thus red shifting the absorption spectra. In Figure 4 it can be seen that this is not occurring and in fact in complexes **40** and **41** the absorption spectra have been blue shifted. An EDG would be expected to raise the level of the LUMO thus blue shifting the absorption spectra which is what is occurring for complex **42**. This leads us to the conclusion that it is not only electronic effects that control the absorption spectra of these complexes but possibly structural changes brought on by the addition of these functional groups.

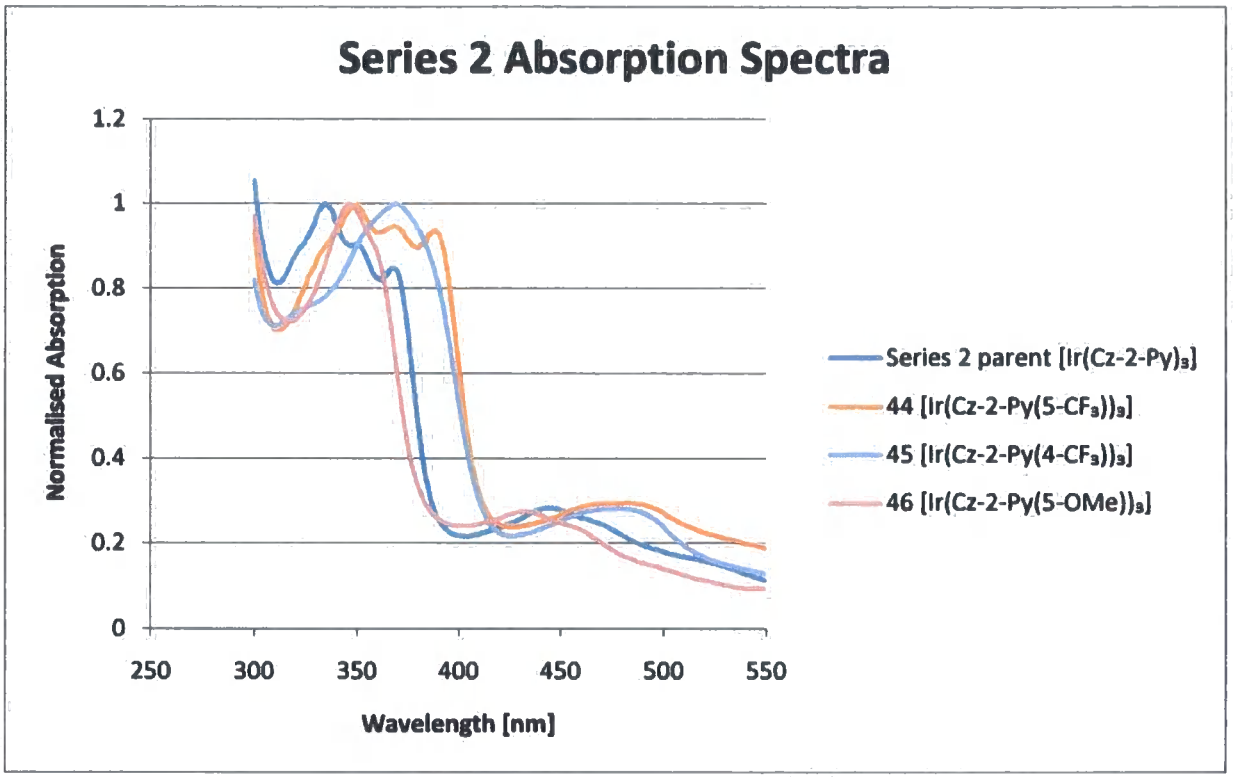

Figure 5 – Normalised absorption spectra of series 2 complexes and their parent complex in degassed toluene at 298 K

Conversely, it can be seen in Figure 5 that for series 2 the absorption spectra of the functionalised complexes have been red shifted relative to the parent complex. This is expected for the EWGs present in complexes **44** and **45** where the level of the LUMO is lowered thus red shifting the absorption spectra. It is not expected for complex **46** where the electron donating methoxy group should raise the level of the LUMO thus blue shifting the absorption spectra, whereas for the actual complex a red shift has been observed.

2.4.2 Emission

The degassed photoluminescence spectra of all complexes synthesised can be seen in Figure 6 (*vide infra*). It should be noted that the lower energy shoulders exhibited by all complexes are typical of vibrational energy levels of mixed MLCT/π-π^* transitions[34].

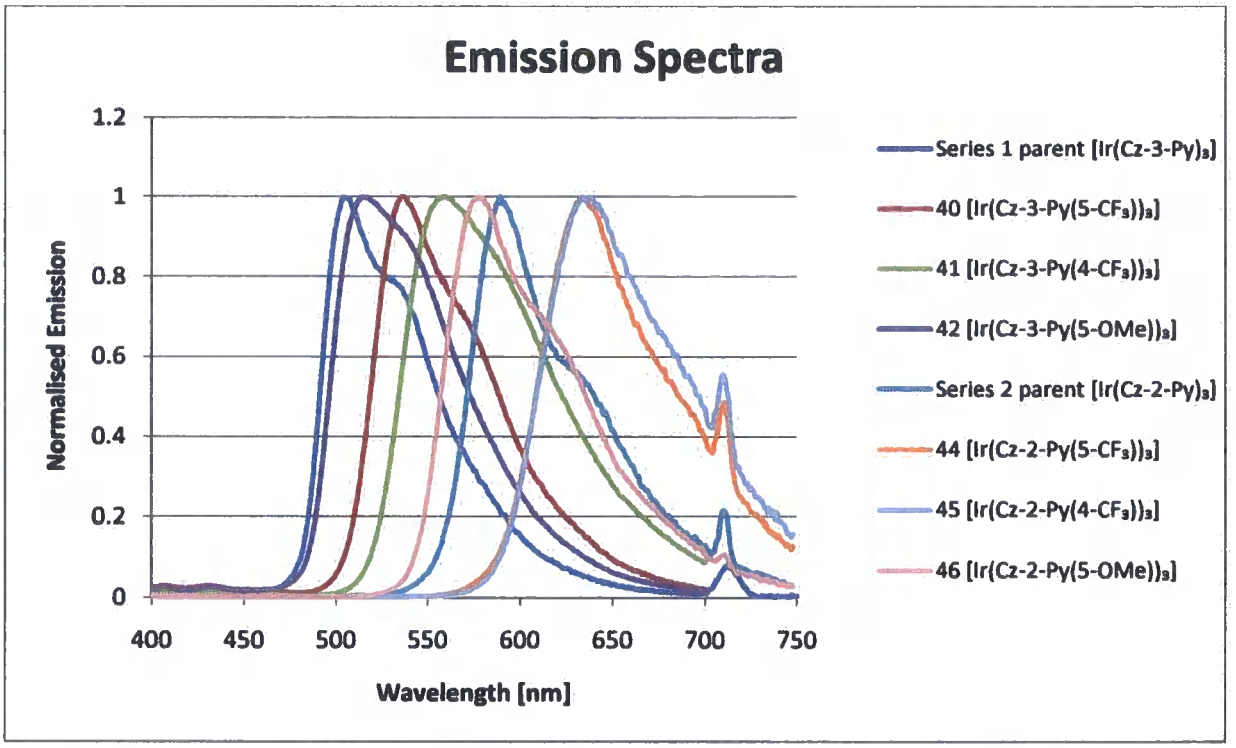

*Figure 6 – Normalised PL spectra for complexes **40, 41, 42, 44, 45, 46** and their parent complexes in degassed toluene at 298 K, λ_{ex} = 355 nm. It should be noted that the peaks at 710 nm are due to the instrument used (double the excitation wavelength)*

From both Table 2 and Figure 6 it can be seen that the emission maxima span a large range from 514 nm (green) to 637 nm (red) covering 123 nm and incorporating several colours of emission over this range. In Figure 7 the emission from several solid state complexes can be seen.

*Figure 7 – Emission from complexes **40, 41 and 42** (left to right) under 365 nm UV light.*

The range of emission of the complexes is relatively large when the visible spectrum range of approximately 380 to 750 nm is considered. As with the original photophysical work performed on

the parent complexes[34] the data is consistent with the emission from a mixed ^{3}MLCT/$^3\pi$-π^* state comprised of mostly ^{3}MLCT character.

A distinct difference can be seen in the emission maxima between series 1 complexes and series 2 complexes. This is analogous to the difference in absorption spectra and CV oxidation values in that it is due to the position of the N in the carbazolyl moiety and the raising of the HOMO level in series 2 thus red shifting the emission.

In both series the complexes containing the CF_3 group (**40**, **41**, **44** and **45**) are all red shifted relative to the parent complex. This is in line with expectations where the electron withdrawing group stabilises the LUMO, lowering its level and reducing the band gap from which emission occurs. The largest shift in emission occurs for complex **41** of 54 nm relative to the parent complex. This is due to a large concentration of LUMO density at the 4-position on the pyridyl moiety where the CF_3 group is located. In turn there is a large effect on the level of the LUMO which is lowered leading to the large red shift observed (504 nm *vs.* 558 nm).

Interestingly the complexes containing the OMe functionalisation (**42** and **46**) exhibit different emission properties. In series 1, complex **42** is slightly red shifted indicating a reduced band gap (504 nm *vs.* 514 nm), opposite of the expected raising of the LUMO level and raising the band gap leading to a blue shift in emission. In series 2, complex **46** follows the expected blue shifted emission with a shift of 12 nm (589 nm *vs.* 577 nm) due to the electron donating effect of the methoxy functionalisation destabilising the LUMO level and resulting in an increased band gap.

2.5 Device Investigation

Preliminary device studies were made by Dr. H. Al-Attar using complex **42** and the parent complex **40**. All devices were fabricated on indium tin oxide (ITO)-coated glass substrates of thickness 125 nm and possessing a sheet resistance of 20 Ω/□. Poly(3,4-ethylenedioxy-thiophene) doped with poly(styrenesulfonic acid) (PEDOT:PSS), obtained commercially from Bayer A.G. Germany, was spin coated at 2500 rpm for 60 sec to produce a ~ 40 nm thick hole-transporting layer (HTL). These HTL-coated substrates were then annealed at 200 °C for 2 min to remove any residual water. A chlorobenzene solution of 20 mg/ml of poly(vinylcarbazole) PVK was selected as a high triplet energy host material and as a hole -transport material. The PVK solution was doped with 40% w/w of 2-(4-biphenylyl)-5-(4-*tert*-butyl-phenyl)-1,3,4-oxadiazole (PBD, **62**, *vide infra*) as an electron transport material for balancing charge carriers transport. Blended devices were made by mixing 8% w/w of the Ir complexes to the PVK:PBD 40% . The prepared mixture was filtered with a 25 µm pore filter and spin coated at 2500 rpm on the top of the PEDOT:PSS layer and baked for 10 min at 120 °C. The

oligomer or the oligomer/polymer solution mixtures were then spin-coated onto the substrate. Each sample was shadow masked to produce two identical devices of area 4x12 mm; the samples were then introduced into a nitrogen glove box, where 4 nm barium cathodes were evaporated onto the device at a rate of ~ 1 Å/s under vacuum at a pressure of *ca.* $1x10^{-6}$ mm Hg. This was followed by the deposition of a 150 nm capping layer of aluminium under the same evaporation conditions.

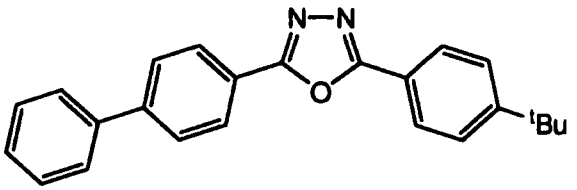

PBD (62)

The current-voltage (*I-V*) characteristics and the emission intensities were measured in a calibrated integrating sphere and the data acquisition were controlled using a home-written NI LabView program which controlled the Agilent Technologies 6632B power supply. The electroluminescence (EL) spectra were measured using an Ocean Optics USB 4000 CCD spectrometer supplied with 400 µm UV/Vis fibre optic. It should be noted that these devices were not optimised and were prepared to investigate the shift in emission between the functionalised complex and the parent complex.

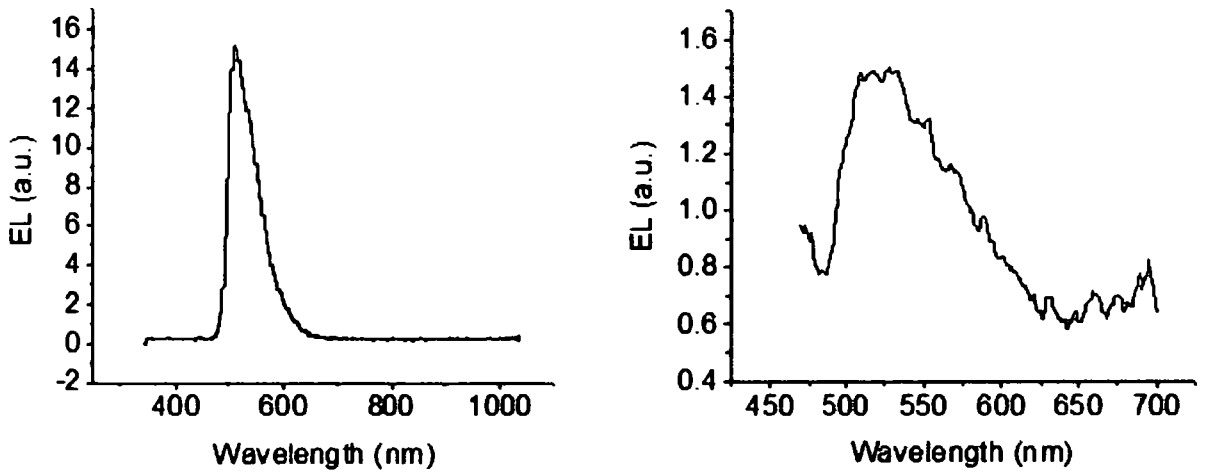

Figure 8 – Comparison of device electroluminescence maxima of complexes 40 (left) and 42 (right)

Figure 8 shows the emission maximum from the parent complex (**40**) to be 511 nm, whilst complex **42** has an emission maximum of 520 nm. The red shifted emission of the functionalised complex was predictable based on the solution photoluminescence spectra where a similar shift was observed. The emission from complex **42** is less defined due to the low external quantum efficiency as demonstrated in Figure 9 below. It should also be noted that there is a difference in dopant

concentration in the devices due to device optimisation. The device containing the parent complex (**40**) has a complex concentration of 10% whereas the device containing the functionalised complex (**42**) has a complex concentration of 20%.

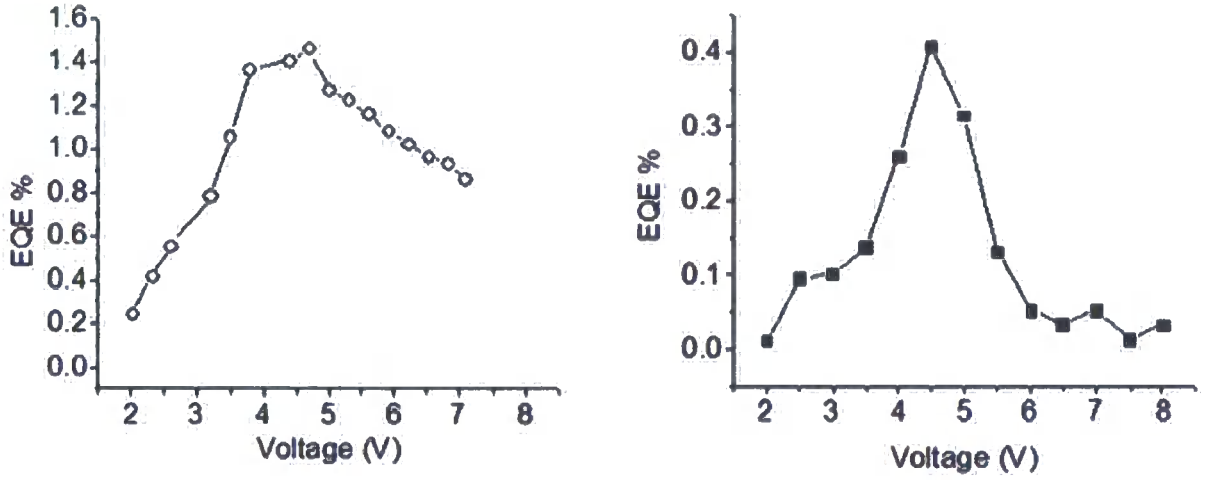

Figure 9 – Comparison of device EQE of complexes 40 (left) and 42 (right)

The relatively low external quantum efficiencies measured are partially as a result of using non-optimised devices. It is envisaged that optimisation of these devices, in particular that of the host materials, could significantly increase the EQE. Investigation is continuing into device optimisation.

It is apparent from Figure 9 that the functionalised complex exhibits lower EQE than the parent complex (0.4% *vs.* 1.5%). This is thought to be due to the presence of a lower energy excited state in the functionalised complex formed through a mixture of the ^{3}MLCT state and the $^3\pi$-π^* state as seen previously[34] which partially decays through non-radiative processes to the ground state. In both complexes the maxima in EQE is attained at approximately 4.5 V, an acceptably low voltage at which to run a device for extended periods in commercialised applications.

2.6 Density Functional Theory Investigation

DFT studies were carried out by Dr. M. Fox. All *ab initio* computations were carried out with the Gaussian 03 package[42]. The model geometries discussed here were optimised using the B3LYP[43, 44, 45, 46] functional with no symmetry constraints. The basis set used was 3-21G*[47, 48]. Frequency calculations were carried out on these optimised geometries at the corresponding levels and shown to have no imaginary frequencies. Molecular orbital and TD DFT computations were carried out on these optimised geometries at the same level of theory. Calculations were carried out on complexes with a methyl group on the carbazole N rather than the hexyl group which was present in the

synthesised complexes. This should not affect the calculated energy levels due to this position playing little importance in the electronic structure of the complexes.

A comparison of the theoretical and experimental absorbance maxima produced from TD-DFT computations on the optimised geometries of model complexes can be seen in Table 3.

The theoretical and experimental data corroborate with each other closely. For example, in both the theoretical and experimental data, complexes **40** and **41** red shift relative to the parent complex. Similarly in series 2 complexes **44** and **45** red shift relative to the parent whereas complex **46** blue shifts relative to the parent, all shifts corroborating the theoretical and experimental agreement.

Complex	Theoretical λ max [nm]	Experimental λ max [nm]
38 Series 1 parent [Ir(Cz-3-Py)$_3$]	395	393
40 [Ir(Cz-3-Py(5-CF_3))$_3$]	430	424
41 [Ir(Cz-3-Py(4-CF_3))$_3$]	436	423
42 [Ir(Cz-3-Py(5-OMe))$_3$]	396	385
39 Series 2 parent [Ir(Cz-2-Py)$_3$]	460	444
44 [Ir(Cz-2-Py(5-CF_3))$_3$]	501	483
45 [Ir(Cz-2-Py(4-CF_3))$_3$]	501	481
46 [Ir(Cz-2-Py(5-OMe))$_3$]	449	432

Table 3 – Comparison of theoretical and experimental absorption data

Schematics showing the computed position and density of the HOMO and LUMO for the parent complexes of series 1 and 2 are shown in Figures 10 and 11 (*vide infra*).

Figure 10 – HOMO (left) and LUMO (right) representations for series 1 parent [Ir(Cz-3-Py)$_3$] with methyl instead of hexyl substituent on carbazole N

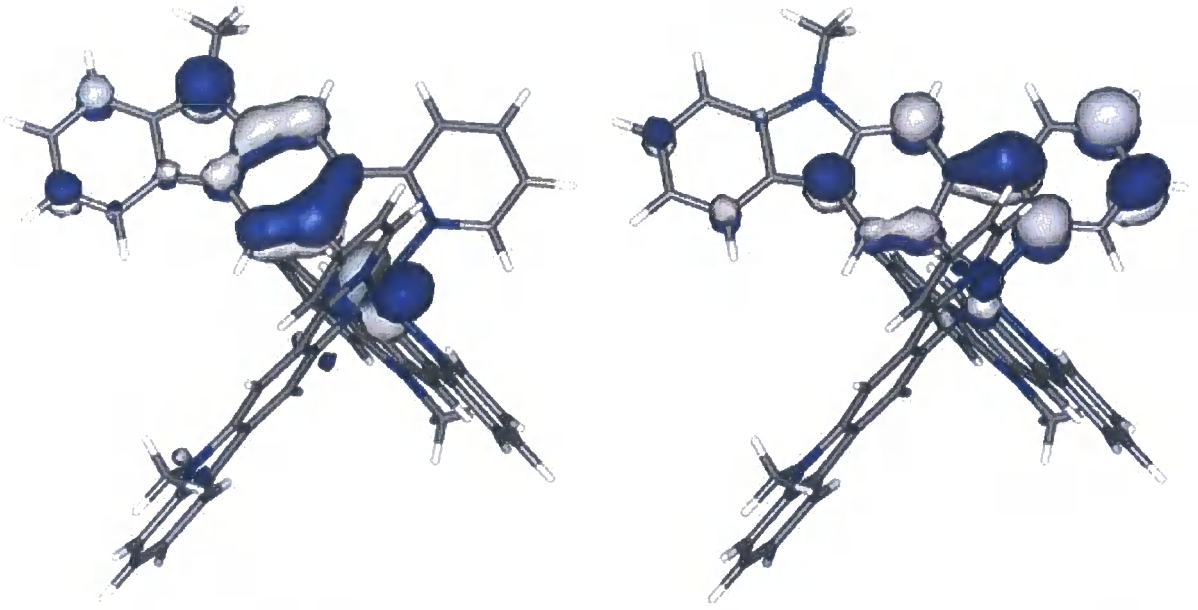

Figure 11 – HOMO (left) and LUMO (right) representations for series 2 parent [Ir(Cz-2-Py)$_3$] with methyl instead of hexyl substituent on carbazole N

It is apparent that for series 1 (Figure 10) there is little carbazole involvement in the HOMO or LUMO compared to series 2 (Figure 11) where much greater carbazole involvement in both HOMO and LUMO can be seen. The resulting increased conjugation in series 2 means the complexes are

stabilised. This is supported in the experimental data where both absorption and emission are red shifted for series 2 relative to series 1. *Vice versa* the decreased carbazole involvement in series 1 destabilises the complexes hence blue shifting the absorption and emission due to the higher energy HOMO-LUMO gap.

The computations also indicate HOMO-LUMO transition in the complexes is primarily from mixed iridium d-orbitals to the ligand π system, *i.e.* a metal to ligand charge transfer state (MLCT). This can be seen in Figures 10 and 11 where the HOMO density is mostly based on the iridium atom, whereas the LUMO density is mostly based on the ligands. The increased HOMO density on the carbazole in series 2 indicates that the HOMO-LUMO transition is more mixed involving both MLCT transitions and a greater influence of π-π^* transitions. In series 1 the HOMO-LUMO transition is also mixed but involves less influence of π-π^* transitions.

Chapter 3 - Experimental

This chapter describes the general experimental procedures and equipment used during the project. The synthesis and characterisation of all the new compounds presented in this thesis are described. The synthesis of several known compounds which were used as precursors is also presented along with the characterisation data used to confirm their identity.

3.1 General Procedures

Reactions that required an inert or dry atmosphere were performed under anhydrous argon which was dried by passage through a column of blue indicating silica gel and phosphorus pentoxide. All reagents were of standard reagent grade and were used as supplied unless otherwise stated from Aldrich, Fluka, Lancaster, Alfa Aesar or Alpha. Where an anhydrous solvent was employed it was dried through an HPLC column on an Innovative Technology Inc. solvent purification system. Petroleum ether refers to the fraction with a boiling point of 40-60 °C. Column chromatography was carried out using silica gel (40-60 μm). Thin layer chromatography was carried out using Polygram SilG/UV F_{254} TLC plates, with visualisation using ultraviolet light (254 or 365 nm). ^{1}H NMR spectra were recorded on either a Bruker Avance 400 at 400MHz or a Varian Inova 500 instrument at 500MHz. ^{13}C NMR spectra were recorded on the above spectrometers at 100 MHz and 125 MHz, respectively. Chemical shifts are reported in ppm downfield of tetramethylsilane (TMS), using TMS or the residual non-deuterated solvent as the internal reference. Electrospray (ES^{+}) mass spectra were recorded on a Micromass LCT mass spectrometer. MALDI-TOF mass spectra were recorded on an Applied Biosystems Voyager-DE STR mass spectrometer. GC-MS mass spectra were recorded on a Thermo-Finnigan Trace mass spectrometer. Melting points were determined using a Stuart Scientific SMP3 melting point apparatus. Elemental analyses were obtained on an Exeter Analytical Inc. CE-440 elemental analyser. DSC studies were performed on a Perkin-Elmer Pyris 1 DSC. TGA studies were performed on a Perkin-Elmer Pyris 1 TGA. Cyclic voltammetric (CV) investigations were carried out on a μ Autolab Type 3 Potentiostat/Galvanostat. Measurements were carried out at 298K using an $Ag/AgNO_3$ reference electrode and the ferrocene/ferrocenium couple[40] as a secondary reference. The supporting electrolyte was a 0.1M solution in DCM of tetra(*n*-butyl)ammonium hexafluorophosphate (nBu_4NPF_6). A scanning rate of 100 mV/s was used.

All devices were fabricated on indium tin oxide (ITO)-coated glass substrates of thickness 125 nm and possessing a sheet resistance of 20 Ω/□. Poly(3,4-ethylenedioxy-thiophene) doped with

poly(styrenesulfonic acid) (PEDOT:PSS), obtained commercially from Bayer A.G. Germany, was spin coated at 2500 rpm for 60 sec to produce a ~ 40 nm thick hole-transporting layer (HTL). These HTL-coated substrates were then annealed at 200 °C for 2 min to remove any residual water. A chlorobenzene solution of 20 mg/ml of poly(vinylcarbazole) PVK was selected as a high triplet energy host material and as a hole -transport material. The PVK solution doped with 40% w/w of 2-(4-biphenylyl)-5-(4-*tert*-butyl-phenyl)-1,3,4-oxadiazole (PBD, **62**) as an electron transport material for balancing charge carriers transport. Blended devices were made by mixing 8% w/w of the Ir complexes to the PVK:PBD 40% . The prepared mixture was filtered with a 25 μm pore filter and spin coated at 2500 rpm on the top of the PEDOT:PSS layer and baked for 10 min at 120 °C. The oligomer or the oligomer/polymer solution mixtures were then spin-coated onto the substrate. Each sample was shadow masked to produce two identical devices of area 4x12 mm; the samples were then introduced into a nitrogen glove box, where 4 nm barium cathodes were evaporated onto the device at a rate of ~ 1 Å/s under vacuum at a pressure of ca. $1x10^{-6}$ mm Hg. This was followed by the deposition of a 150 nm capping layer of aluminium under the same evaporation conditions.

The current-voltage (*I-V*) characteristics and the emission intensities were measured in a calibrated integrating sphere and the data acquisition were controlled using a home-written NI LabView program which controlled the Agilent Technologies 6632B power supply. The electroluminescence (EL) spectra were measured using an Ocean Optics USB 4000 CCD spectrometer supplied with 400 μm UV/Vis fibre optic. It should be noted that these devices were not optimised and were prepared to investigate the shift in emission between the functionalised complex and the parent complex.

Solution state photophysical properties were ascertained using freshly prepared solutions of the available complexes in toluene. Emission measurements were taken using solutions which were degassed thoroughly using the repeated freeze-thaw technique. All measurements were taken using 1 cm pathlength quartz cuvettes. Series 1 absorption measurements were taken using a Unicam UV/Vis Spectrometer UV2. Series 2 absorption measurements were taken using a Perkin Elmer UV/Vis Spectrometer Lambda12. All emission measurements were taken using a Jobin-Yvon Horiba Spex Fluorolog Spectrometer.

3.2 Experimental Procedures

Preparation of 2-chloro-4-methoxypyridine (63)[49]

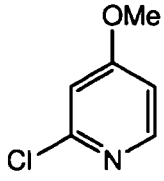

(63)

An argon-filled flame-dried flask was charged with 2-chloro-4-nitropyridine (3.00 g, 18.9 mmol) which was dissolved in anhydrous THF (20 ml). To this solution tetrabutylammonium methoxide (6.4 ml, 19.9 mmol) was added and the solution was stirred for 65 h at room temperature. After this time the solution was diluted with distilled H_2O and the organic and aqueous layers were separated. The organic products were extracted with DCM (4x30 ml) and dried ($MgSO_4$). The solvent was removed *in vacuo* leaving the crude product as a yellow solid. This was purified by columm chromatography on silica using an eluent of DCM:EtOAc (10:1 v/v) isolating **63** (1.06 g, 39%) as clear yellow liquid.

^{1}H NMR (400 MHz, $CDCl_3$) δ_H 8.17 (1H, d, *J* 5.8, H-6), 6.82 (1H, d, *J* 2.3, H-3), 6.73 (1H, dd, *J* 2.3, 5.8, H-3), 3.84 (3H, s, OMe).

Preparation of 3-bromo-9-hexyl-9H-carbazole (64)[33]

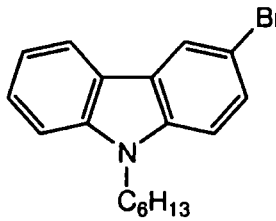

(64)

An argon-filled flame-dried flask was charged with 3-bromo-9H-carbazole (1.05 g, 4.27 mmol) and potassium *tert*-butoxide (0.62 g, 5.53 mmol) to which anhydrous DMF (25 ml) was added. The solution was stirred for 2 h at room temperature. After this time 1-bromohexane (1.18 g, 7.16 mmol) was added to the flask which was heated to 130 °C for 65 h. The reaction was quenched with distilled H_2O and the organic products extracted with DCM (4x30 ml) and dried ($MgSO_4$). The DCM was removed *in vacuo* to give a light yellow oil as the crude product. This was purified by column chromatography on silica using an eluent of petroleum ether:DCM (9:1 v/v) to give **64** (1.30 g, 92%) as a clear colourless oil.

^{1}H NMR (400 MHz, $CDCl_3$) δ_H 8.20 (1H, s, H-4), 8.04 (1H, dd, *J* 7.5, 1.4, H-2), 7.55-7.21 (5H, m), 4.25 (2H, td, *J* 7.3, 2.3, NH_2CH_2), 1.85 (2H, m, NCH_2CH_2), 1.41-0.80 (9H, m).

Preparation of 9-hexyl-9H-carbazol-3-yl-3-boronic acid (61)[33]

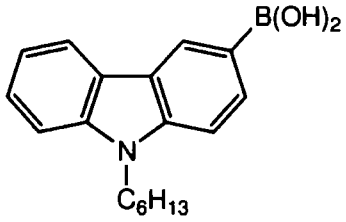

(61)

An argon-filled flame-dried flask was charged with **64** (5.14 g, 15.56 mmol) which was dissolved in anhydrous THF (100 ml) cooled to -78 °C. *n*-BuLi (1.6 M in hexane, 7.5 ml, 18.67 mmol) was added dropwise over 2 h and the solution was stirred for a further 1 h at -78 °C. Triisopropylborate (10.77 ml, 46.68 mmol) was added to the solution which was stirred for 22 h whilst warming from -78 °C to room temperature. After this time HCl (4 M, 18.3 ml, 73.13 mmol) was added to the solution which turned from a light yellow colour to a dark green colour. The solution was stirred for 2 h by which point it was a dark yellow colour. Na_2CO_3 solution (2 M) was added until the solution was neutralised and a light yellow colour. The organic and aqueous layers were separated and the organic products were extracted with DCM (4x30 ml) and dried ($MgSO_4$). The solvents were removed in vacuo to give a light brown solid as the crude product. This was purified by column chromatography on silica using a graduated eluent system of DCM followed by DCM:EtOAc (1:1 v/v) and then DCM:EtOAc:MeOH (5:5:1 v/v) to give **61** (2.90 g, 63%) as a white solid.

^{1}H NMR (400 MHz, $CDCl_3$) δ_H 9.11 (1H, s, H-4), 8.47 (1H, dd, *J* 8.2, 1.1, H-2), 8.34 (1H, d, *J* 7.4, H-3), 7.59-7.46 (3H, m), 7.38-7.34 (1H, m), 4.37 (2H, t, *J* 7.2, NCH_2), 1.89-1.84 (2H, m), 1.44-1.23 (6H, m), 0.90 (3H, t, *J* 6.9, CH_3).

^{13}C NMR (101 MHz, $CDCl_3$) δ_C 143.67, 140.91, 133.28, 128.96, 125.96, 123.50, 123.03, 120.90, 119.60, 109.08, 108.45, 43.45, 31.83, 29.19, 27.24, 22.79, 14.25.

Preparation of 3-[5-(trifluoromethyl)pyridin-2-yl]-9-hexyl-9H-carbazole (65)

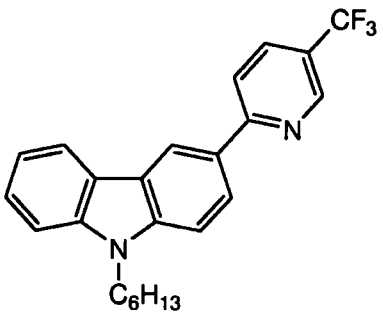

(65)

An argon-filled flask was charged with **61** (0.56 g, 1.90 mmol) which was dissolved in degassed toluene (40 ml). Na_2CO_3 solution (2 M, 9.7 ml, 19.38 mmol), bis(triphenylphosphine)palladium(II) dichloride (0.08 g, 0.11 mmol) and 2-chloro-5-trifluoromethylpyridine (0.86 g, 4.75 mmol) were added to the solution which was heated at 90 °C for 65 h. After this time the solution was diluted with distilled H_2O (50 ml) and the organic products were extracted with DCM

(4x30 ml) and dried ($MgSO_4$). The solvent was removed in vacuo to give an orange coloured oil as the crude product. This was purified by column chromatography on silica using a graduated eluent system of hexane followed by petroleum ether:DCM (4:1 v/v) and then petroleum ether:DCM (1:1 v/v) to give **65** (0.53 g, 71%) as an off white solid; mp 88-89 °C.

Found: C, 72.8; H, 5.9; N, 7.0. Calc. for $C_{24}H_{23}F_3N_2$: C, 72.7; H, 5.85; N, 7.1.

^{1}H NMR (500 MHz, C_6D_6) δ_H 8.98 (1H, s), 8.93 (1H, d, *J* 1.6), 8.39 (1H, dd, *J* 8.6, 1.8), 8.11 (1H, d, *J* 7.7), 7.44-7.37 (2H, m), 7.30 (1H, d, *J* 8.4), 7.26 (1H, t, *J* 7.1), 7.22 (1H, d, *J* 8.6), 7.16 (1H, t, *J* 4.0), 3.76 (2H, t, *J* 7.2, NCH_2), 1.53-1.44 (2H, m, NCH_2CH_2), 1.14-0.98 (6H, m), 0.79 (3H, t, *J* 7.1, CH_3).

^{13}C NMR (126 MHz, C_6D_6) δ_C 161.88, 147.05, 142.44, 141.83, 133.88, 129.70, 126.77, 125.98, 124.21, 124.06, 123.96, 121.36, 120.53, 120.26, 119.37, 109.72, 109.58, 43.39, 32.10, 29.40, 27.44, 23.15, 14.52.

GC-MS (EI) *m/z* = 325 (M^+ - C_5H_{11}, 100%), 396 (M^+, 71).

Preparation of 3-(4-(trifluoromethyl)pyridin-2-yl)-9-hexyl-9H-carbazole (66)

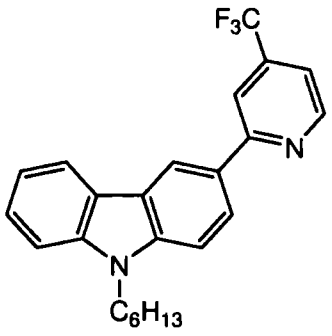

(66)

An argon-filled flask was charged with **61** (0.50 g, 1.69 mmol) which was dissolved in 35ml of degassed toluene (35 ml). To this solution Na_2CO_3 solution (2 M, 9.7 ml, 19.38 mmol), bis(triphenylphosphine)palladium(II) dichloride (0.08 g, 0.11 mmol) and 2-chloro-4-trifluoromethylpyridine (0.29 g, 1.61 mmol) were added and the solution was heated at 90 °C for 65 h. Workup as described for **65** gave a dark brown oil as the crude product. This was purified by column chromatography on silica using an eluent of hexane:DCM (1:1 v/v) to give **66** (0.42 g, 66%) as a light yellow solid; mp 74-75 °C.

Found: C, 72.5; H, 5.9; N, 7.0. Calc. for $C_{24}H_{23}F_3N_2$: C, 72.7; H, 5.85; N, 7.1.

^{1}H NMR (400 MHz, $CDCl_3$) δ_H 8.88 (1H, d, *J* 5.0), 8.81 (1H, d, *J* 1.7), 8.20 (1H, d, *J* 7.9), 8.17 (1H, dd, *J* 8.4, 1.8) 8.06 (1H, s), 7.51-7.48 (2H, m), 7.45-7.05 (2H, m), 7.28 (1H, td, *J* 7.4, 1.1), 4.34 (2H, t, *J* 7.3, NCH_2), 1.96-1.88 (2H, m, NCH_2CH_2), 1.44-1.33 (6H, m), 0.86 (3H, t, *J* 6.8, CH_3).

^{13}C NMR (101 MHz, $CDCl_3$) δ_C 147.05, 142.30, 141.87, 141.28, 126.38, 125.05, 123.72, 123.29, 123.22, 120.92, 119.71, 119.67, 109.32, 109.26, 43.54, 31.13, 29.17, 27.18, 22.74, 14.20.

GC-MS (EI) *m/z* = 325 (M^+ - C_5H_{11}, 100%), 396 (M^+, 71).

Preparation of 9-hexyl-3-(5-methoxypyridin-2-yl)-9H-carbazole (67)

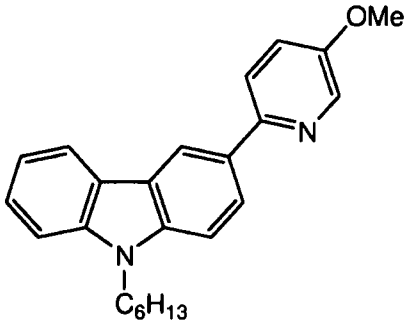

(**67**)

An argon-filled flask was charged with **61** (0.51 g, 1.73 mmol) which was dissolved in degassed toluene (35 ml). To this solution Na_2CO_3 solution (2 M, 9.7 ml, 19.38 mmol), bis(triphenylphosphine)palladium(II) dichloride (0.08 g, 0.11 mmol) and 2-bromo-5-methoxypyridine (0.80 g, 4.23 mmol) were added and the solution was heated at 90 °C for 65 h. After this time the solution was diluted with distilled H_2O (50 ml) and the organic products were extracted with EtOAc (4x30 ml) and dried ($MgSO_4$). The solvent was removed in vacuo. The crude product was purified by column chromatography on silica using an eluent of DCM:EtOAc (20:1 v/v) giving an impure product as an orange oil. This was distilled using a Kugelrohr apparatus to give **67** (0.27 g, 44%) as a light orange oil.

Found: C, 80.1; H, 7.4; N, 7.5. Calc. for $C_{24}H_{26}N_2O$: C, 80.4; H, 7.3; N, 7.8.

^1H NMR (400 MHz, $CDCl_3$) δ_H 8.74 (1H, s), 8.46 (1H, d, *J* 3.0), 8.21 (1H, d, *J* 7.8), 8.05 (1H, dd, *J* 8.6, 1.1), 7.68 (1H, d, *J* 8.7), 7.48 (1H, t, *J* 7.6), 7.41-7.38 (2H, m), 7.28 (1H, t, *J* 7.4), 7.18 (1H, dd, *J* 8.7, 2.9), 4.22 (2H, t, *J* 7.2, NCH_2), 3.80 (3H, s, OCH_3), 1.88 – 1.77 (2H, m, NCH_2CH_2), 1.32-1.25 (6H, m), 0.88 (3H, t, *J* 6.9, CH_3).

^{13}C NMR (101 MHz, $CDCl_3$) δ_C 154.27, 151.10, 140.98, 140.64, 136.86, 130.23, 125.78, 124.45, 123.31, 123.24, 121.48, 120.42, 119.02, 118.43, 108.88, 108.82, 55.59, 43.13, 31.60, 28.97, 26.97, 22.57, 14.05.

MS (ES^+) *m/z* = 359 (M^+, 100%)

Preparation of 9-hexyl-3-(4-methoxypyridin-2-yl)-9H-carbazole (68)

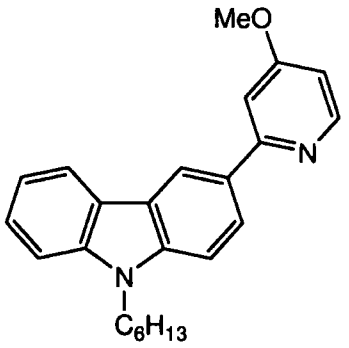

(**68**)

An argon-filled flask was charged with **61** (0.50 g, 1.69 mmol) which was dissolved in degassed toluene (40 ml). To this solution Na_2CO_3 solution (2 M, 9.7 ml, 19.38 mmol), bis(triphenylphosphine)palladium(II) dichloride (0.08 g, 0.11 mmol) and **63** (0.23 g, 1.61 mmol) were added and the solution was heated at 90 °C for 65 h. Work-up as described for **67** gave a crude product which was purified by column chromatography on silica using an eluent of DCM:EtOAc (9:1 v/v) to give **68** (0.21 g, 36%) as a light orange oil.

^{1}H NMR (400 MHz, $CDCl_3$) δ_H 8.76 (1H, dd, *J* 1.8, 0.5), 8.58 (1H, d, *J* 5.7), 8.21 (1H, d, *J* 7.5), 8.12 (1H, dd, *J* 8.6, 1.8), 7.54-7.42 (3H, m), 7.38 (1H, d, *J* 2.2), 7.31-7.25 (1H, m), 6.79 (1H, dd, *J* 5.7, 2.4), 4.35 (2H, t, *J* 7.2, NCH_2), 3.97 (3H, s, OCH_3), 1.95-1.88 (2H, m, NCH_2CH_2), 1.47-1.24 (6H, m), 0.89 (3 H, t, *J* 7.1, CH_3).

^{13}C NMR (101 MHz, $CDCl_3$) δ_C 166.64, 160.32, 150.97, 141.35, 141.17, 130.60, 126.02, 125.04, 123.41, 120.83, 119.38, 119.30, 109.07, 108.93, 107.57, 106.51, 55.36, 43.45, 31.78, 29.17, 27.17, 22.74, 14.20.

MS (ES^+) *m/z* = 359 (M^+, 100%).

Preparation of *fac*-{3-[5-(trifluoromethyl)pyridin-2-yl]-9-hexyl-9H-carbazole}$_3$Iridium^{III} (40)

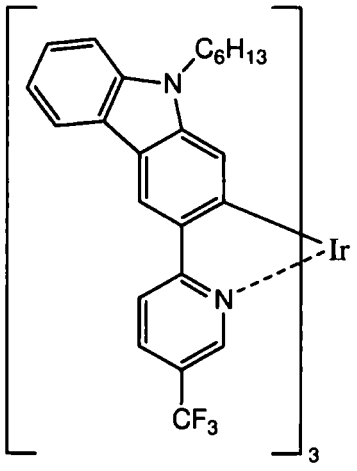

(**40**)

An argon-filled flask was charged with **65** (0.47 g, 1.19 mmol) and Ir(acetylacetonate)$_3$ (0.12 g, 0.25 mmol) which were dissolved in degassed glycerol (15 ml). The solution was heated at 220 °C for 65 h then it was allowed to cool to room temperature and diluted with distilled H_2O (50 ml) and brine solution. The organic products were extracted with DCM (4x30 ml) and dried ($MgSO_4$). The solvent was removed *in vacuo* to give a dark orange oil as the crude product. This was purified by column chromatography on silica using hexane:DCM (1:1 v/v) to give **40** (0.08 g, 8%) as a light yellow powder; mp 333 °C.

^{1}H NMR (400 MHz, $CDCl_3$) δ_H 8.47 (3H, s), 8.13 (3H, d, *J* 8.6), 8.03 (3H, d, *J* 7.6), 7.84-7.74 (6H, m), 7.32 (3H, t, *J* 7.5), 7.17-7.12 (6H, m), 6.74 (3H, s), 3.76-3.63 (6H, m, NCH_2), 1.42-1.37 (6H, m, NCH_2CH_2), 0.88-0.75 (18H, m), 0.63 (9H, t, *J* 6.5, CH_3).

^{13}C NMR (101 MHz, $CDCl_3$) δ_C 170.66, 160.35, 144.60, 140.52, 134.30, 133.35, 129.02, 124.73, 124.38, 123.82, 123.49, 121.94, 119.19, 118.27, 118.24, 118.12, 115.69, 108.71, 42.91, 31.45, 28.53, 26.86, 22.44, 14.10.

MS (MALDI-TOF) *m/z* = 1379 (M^+, 100%).

Preparation of *fac*-{3-[4-(trifluoromethyl)pyridin-2-yl]-9-hexyl-9H-carbazole}$_3$Iridium^{III} (41)

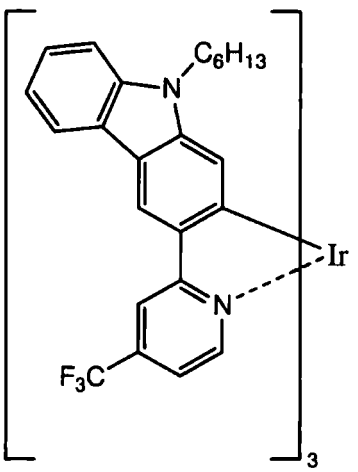

(**41**)

An argon-filled flask was charged with **66** (0.40 g, 1.01 mmol) and Ir(acetylacetonate)$_3$ (0.12 g, 0.25 mmol) which were dissolved in degassed glycerol (15 ml). Following the procedure described for **40**, a dark orange oil was obtained as the crude product. This was purified by column chromatography on silica using hexane:DCM (1:1 v/v) to give **41** (0.02 g, 2%) as a bright orange powder; mp 328 °C.

^{1}H NMR (500 MHz, CD_2Cl_2) δ_H 8.53 (3H, s), 8.30 (3H, s), 8.06 (3H, d, *J* 7.6), 7.91 (3H, d, *J* 5.8), 7.34 (3H, t, *J* 7.7), 7.20 (3H, d, *J* 8.2), 7.15 (3H, t, *J* 7.5), 7.06 (3H, dd, *J* 5.8, 1.6), 6.73 (3H, s), 3.78-3.63 (6H, m,

NCH_2), 1.41-1.36 (6H, m, NCH_2CH_2), 0.93-0.84 (12H, m), 0.83-0.76 (6H, t, *J* 16.6), 0.65 (9H, t, *J* 6.8).

^{13}C NMR (126 MHz, CD_2Cl_2) δ_C 168.97, 160.07, 148.89, 144.67, 140.75, 138.33, 134.93, 124.95, 124.60, 123.60, 119.45, 118.19, 117.88, 116.95, 116.06, 114.88, 109.10, 43.17, 31.78, 28.86, 27.22, 22.80, 14.17.

MS (MALDI-TOF) *m/z* = 1379 (M^+, 100%).

Preparation of *fac*-{9-hexyl-3-[5-methoxypyridin-2-yl]-9H-carbazole}$_3$Iridium^{III} (42)

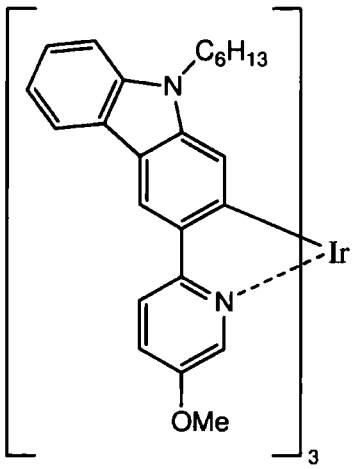

(**42**)

An argon-filled flask was charged with **67** (0.27 g, 0.75 mmol) and Ir(acetylacetonate)$_3$ (0.11 g, 0.21 mmol) which were dissolved in degassed glycerol (15 ml). Following the procedure described for **40** a green solid was obtained as the crude product. This was purified by column chromatography on silica using hexane:DCM (1:1 v/v) to give **42** (0.07 g, 8%) as a bright yellow/green powder; mp 355 °C.

^1H NMR (500 MHz, CD_2Cl_2) δ_H 8.33 (3H, s), 8.03-8.01 (6H, m), 7.44 (3H, d, *J* 2.7), 7.33-7.25 (6H, m), 7.16 (3H, d, *J* 8.1), 7.09 (3H, t, *J* 7.4), 6.79 (3H, s), 3.75-3.68 (6H, m, NCH_2), 3.66 (9H, d, *J* 9.6, OCH_3), 1.42-1.36 (6H, m, NCH_2CH_2), 0.94-0.85 (12H, m), 0.84-0.77 (6H, m), 0.65 (9H, t, *J* 6.8, CH_3).

^{13}C NMR (126 MHz, CD_2Cl_2) δ_C 160.75, 158.99, 154.91, 143.44, 140.46, 136.87, 134.89, 124.86, 124.05, 121.99, 119.11, 119.08, 118.63, 117.18, 115.88, 115.35, 108.70, 56.12, 43.10, 31.81, 28.90, 27.21, 22.81, 14.26.

MS (MALDI-TOF) *m/z* = 1265 (M^+, 100%).

Attempted preparation of *fac*-{9-hexyl-3-[4-methoxypyridin-2-yl]-9H-carbazole}$_3$Iridium^{III} (43)

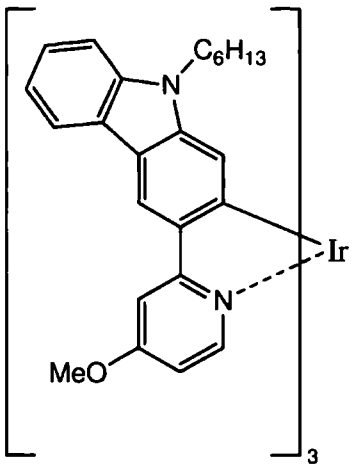

(43)

An argon-filled flask was charged with **68** (0.58 g, 1.62 mmol) and Ir(acetylacetonate)$_3$ (0.23 g, 0.46 mmol) which were dissolved in degassed glycerol (20 ml). Following the procedure described for **40** gave a dark oil. Thin layer chromatography showed a multi-component product mixture from which the desired product **43** could not be isolated.

Preparation of 4-bromo-2-nitrobiphenyl (53)[33]

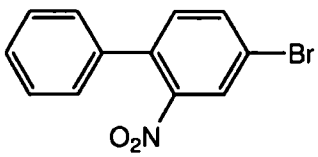

(53)

An argon-filled flask was charged with phenylboronic acid (5.00 g, 41.01 mmol) and 1,4-dibromo-2-nitrobenzene (11.52 g, 41.01 mmol) which were dissolved in degassed toluene (125 ml). To this solution Na_2CO_3 solution (2 M, 61.5 ml, 123.0 mmol) and bis(triphenylphosphine)palladium(II) dichloride (0.86 g, 1.23 mmol) were added and the solution was heated at 90 °C for 5.5 h. After this time the solution was allowed to cool to room temperature then diluted with distilled H_2O (50 ml). The organic and aqueous phases were separated and the organic products extracted with DCM (4x30 ml) and dried with $MgSO_4$. The solvents were removed *in vacuo* to give a dark brown liquid as the crude product. This was purified by column chromatography on silica using a short column and an eluent of hexane:DCM (1:1 v/v) to give a mixture of **53** and 4-phenyl-2-nitrobiphenyl (**54**) as a clear yellow liquid (11.50 g). From NMR data it was calculated that 77% of the mixture was **53** (8.86 g, 78%).

^{1}H NMR (400 MHz, $CDCl_3$) δ_H 7.97 (1H, d, *J* 2.2), 7.74 (1H, d, *J* 2.0), 7.72 (1H, d, *J* 2.0), 7.58 (1H, s), 7.55 (1H, d, *J* 2.2), 7.29-7.25 (3H, m).

Preparation of 2-bromo-9H-carbazole (49)[33]

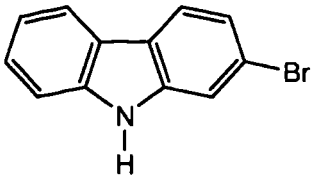

(49)

An argon-filled flask was charged with **53** (7.52 g, 27.04 mmol) which was dissolved in triethylphosphite (30.5 ml, 189.3 mmol). The solution was heated at 160 °C for 10 h. After this time the triethylphosphite was removed *in vacuo* at 90 °C resulting in a dark residue to which a mixture of MeOH:H_2O (200 ml, 1:1 v/v) was added giving a brown precipitate. The precipitate was filtered and washed with MeOH:H_2O (1:1 v/v) and was found from NMR data to contain **49** and 2-phenyl-9H-carbazole (**55**) in a 9:1 ratio, respectively (3.25 g, 49%). This mixture was used in the next step without further purification.

^{1}H NMR (400 MHz, DMSO-d_6) δ_H 11.39 (1H, s, NH), 8.12 (1H, d, *J* 8.0), 8.07 (1H, d, *J* 8.0), 7.66 (1H, s, H-1), 7.51 (1H, d, *J* 8.2), 7.41 (1H, t, *J* 8.2), 7.29 (1H, d, *J* 8.2), 7.18 (1H, t, *J* 8.2).

MS (EI) *m/z* = 74 (100%), 245 (M^+ [^{79}Br], 11), 247 (M^+ [^{81}Br], 10).

Preparation of 2-bromo-9-hexyl-9H-carbazole (69)[33]

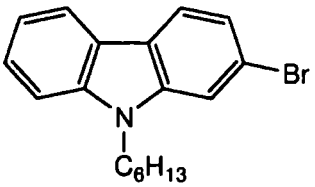

(69)

An argon-filled flame-dried flask was charged with crude **49** (3.25 g, 13.21 mmol) and potassium *tert*-butoxide (1.78 g, 15.85 mmol) to which anhydrous DMF (75 ml) was added. The solution was stirred for 2 h at room temperature. After this time 1-bromohexane (3.25 g, 19.82 mmol) was added to the flask which was heated to 130 °C for 65 h. The reaction was quenched with distilled H_2O (50 ml) and the organic products were extracted with DCM (4x30 ml) and dried ($MgSO_4$). The DCM was removed *in vacuo* to give a dark brown oil as the crude product. This was purified by column chromatography on silica using as eluent of hexane:DCM (9:1 v/v) to give **69** (3.44 g, 79%) as a clear colourless oil.

^{1}H NMR (400 MHz, $CDCl_3$) δ_H 8.04 (1H, d, *J* 8.2), 7.92 (1H, d, *J* 8.2), 7.52 (1H, s), 7.46 (1H, t, *J* 8.2), 7.38 (1H, d, *J* 8.2), 7.30 (1H, d, *J* 8.2), 7.21 (1H, t, *J* 8.2), 4.23 (2H, t, *J* 7.3, NCH_2), 1.87-1.80 (2H, m, NCH_2CH_2), 1.42-1.22 (6H, m), 0.85 (3 H, t, *J* 7.1, CH_3).

Preparation of 9-hexyl-9H-carbazol-2-yl-2-boronic acid (60)[33]

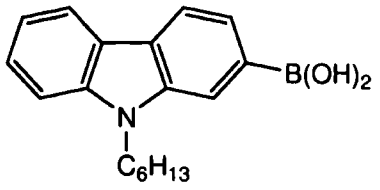

(60)

An argon-filled flame-dried flask was charged with **69** (7.10 g, 21.50 mmol) which was dissolved in anhydrous THF (100 ml) cooled to -78 °C. *n*-BuLi in hexane (2.5 M, 10.3 ml, 25.80 mmol) was added dropwise over 2 h and the solution was stirred for 1 h at -78 °C. Triisopropylborate (9.9 ml, 64.50 mmol) was added to the solution which was stirred for 16 h whilst warming from -78 °C to room temperature. After this time HCl (4 M, 18 ml, 107.5 mmol) was added to the solution. The solution was stirred for 2 h at which point Na_2CO_3 solution (2 M) was added until the solution was neutralised. The organic and aqueous layers were separated and the organic products were extracted with DCM (4x30 ml) and dried ($MgSO_4$). The solvents were removed *in vacuo* to give a light brown solid as the crude product. This was purified by column chromatography on silica using a graduated eluent system of DCM:EtOAc (1:1 v/v) followed by DCM:EtOAc:MeOH (5:5:1 v/v) to give a mixture of **60** and the boronic ester of **60** (3.65 g, 58%) as a white solid. This mixture was converted to the boroxine derivative for elemental analysis by heating the solid in a flask in an oven at 100 °C for 16 h.

Found: C, 77.9; H, 7.2; N, 5.0. Calc. for $C_{54}H_{60}B_3N_3O_3$: C, 78.0; H, 7.3; N, 5.05.

^{1}H NMR δ_H (400 MHz, $CDCl_3$) 8.36 (1H, s), 8.27 (1H, d, *J* 7.8), 8.21-8.18 (2H, m), 7.53 (1H, t, *J* 7.8), 7.46 (1H, d, *J* 7.8), 7.27 (1H, t, *J* 7.8), 4.45 (2H, t, *J* 7.2, NCH_2), 2.06-1.94 (2H, m, NCH_2CH_2), 1.57-1.22 (6H, m), 0.89 (3H, t, *J* 7.2, CH_3).

Preparation of 2-[5-(trifluoromethyl)pyridin-2-yl]-9-hexyl-9H-carbazole (70)

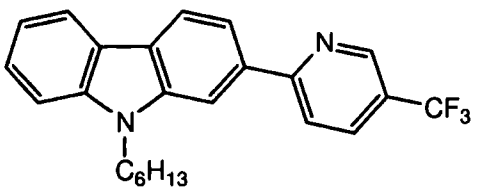

(70)

An argon-filled flask was charged with **60** (1.00 g, 3.39 mmol) which was dissolved in degassed toluene (150 ml). To this solution Na_2CO_3 solution (2 M, 4.13 g, 38.99 mmol), tetrakis(triphenylphosphine)palladium(0) (0.25 g, 0.22 mmol) and 2-chloro-5-trifluoromethylpyridine (0.59 g, 3.22 mmol) were added and the solution was heated at 90 °C for 96 h. After this time the solution was diluted with distilled H_2O (50 ml) and the organic products were extracted with DCM (4x30 ml) and dried ($MgSO_4$). The solvent was removed *in vacuo* to give an orange liquid as the crude product. This

was purified by column chromatography on silica using an eluent of petroleum ether:DCM (1:1 v/v) to give **70** (0.70 g, 55%) as an off-white/yellow solid; mp 112-113 °C.

Found: C, 72.7; H, 5.8; N, 7.0. Calc. for $C_{24}H_{23}F_3N_2$: C, 72.7; H, 5.9; N, 7.1.

^{1}H NMR (400 MHz, $CDCl_3$) δ_H 8.97 (1H, s), 8.18-8.16 (2H, m), 8.12 (1H, d, *J* 7.7), 8.02-7.94 (2H, m), 7.82 (1H, dd, *J* 8.3, 1.4), 7.49 (1H, dt, *J* 8.2, 1.2), 7.42 (1H, d, *J* 8.2), 7.28-7.21 (1H, m), 4.38 (2H, t, *J* 7.3, NCH_2), 1.96-1.85 (2H, m, NCH_2CH_2), 1.46-1.23 (6H, m), 0.84 (3H, t, *J* 7.1, CH_3).

^{13}C NMR (101 MHz, $CDCl_3$) δ_C 161.67, 146.78, 141.71, 141.10, 135.52, 134.05, 126.61, 124.66, 124.65, 124.12, 122.57, 121.01, 120.87, 120.42, 119.36, 118.17, 109.18, 108.01, 43.40, 31.81, 29.24, 27.19, 22.77, 14.22.

GC-MS (EI) *m/z* = 55 (100%), 146 (M^+ - $C_{18}H_{20}N$, 46), 325 (M^+ - C_5H_{11}, 29), 396 (M^+, 8).

Preparation of 2-[4-(trifluoromethyl)pyridin-2-yl]-9-hexyl-9H-carbazole (71)

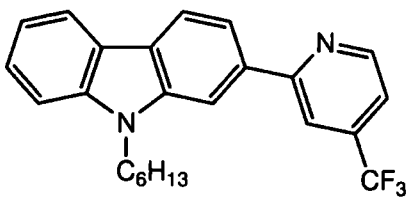

(71)

An argon-filled flask was charged with **60** (1.00.g, 3.39.mmol) which was dissolved in degassed toluene (150 ml). To this solution Na_2CO_3 solution (2 M, 4.13 g, 38.99 mmol), tetrakis(triphenylphosphine)palladium(0) (0.25 g, 0.22 mmol) and 2-chloro-4-trifluoromethylpyridine (0.59 g, 3.24 mmol) were added. Following the procedure described for **70** gave a yellow liquid as the crude product. This was purified by column chromatography on silica using an eluent of petroleum ether:DCM (1:1 v/v) to give **71** (0.78 g, 61%) as a white powder; mp 120-121 °C.

Found: C, 72.7; H, 5.9; N, 7.1. Calc. for $C_{24}H_{23}F_3N_2$: C, 72.7; H, 5.9; N, 7.1.

^{1}H NMR (400 MHz, $CDCl_3$) δ_H 8.89 (1H, d, *J* 5.0), 8.20-8.10 (3H, m), 8.05 (1H, s), 7.83 (1H, dd, *J* 8.2, 1.5), 7.49 (1H, td, *J* 8.2, 1.2), 7.45-7.41 (2H, m), 7.27-7.22 (1H, m), 4.38 (2H, t, *J* 7.3, NCH_2), 1.98-1.83 (2H, m, NCH_2CH_2), 1.46-1.21 (6H, m), 0.85 (3H, t, *J* 7.1, CH_3).

^{13}C NMR (101 MHz, $CDCl_3$) δ_C 159.83, 150.79, 141.67, 141.13, 139.31, 135.69, 126.53, 124.48, 123.30, 122.59, 120.99, 120.91, 119.34, 118.00, 117.36, 116.54, 109.16, 107.71, 43.38, 31.80, 29.23, 27.18, 22.77, 14.21.

GC-MS (EI) *m/z* = 325 (M^+ - C_5H_{11}, 100%), 396 (M^+, 58).

Preparation of 9-hexyl-2-(5-methoxypyridin-2-yl)-9H-carbazole (72)

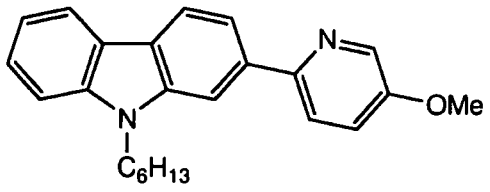

(72)

An argon-filled flask was charged with **60** (1.00 g, 3.39 mmol) which was dissolved in degassed toluene (150 ml). To this solution Na_2CO_3 solution (2 M, 4.13 g, 38.99 mmol), tetrakis(triphenylphosphine)palladium(0) (0.25 g, 0.22 mmol) and 2-bromo-5-methoxypyridine (0.60 g, 3.17 mmol) were added. Following the procedure described for **70** gave a dark orange oil as the crude product. This was purified by column chromatography on silica using an eluent of DCM to give **72** (0.52 g, 46%) as a white solid; mp 117-118 °C.

Found: C, 80.3; H, 7.3; N, 7.9. Calc. for $C_{24}H_{26}N_2O$: C, 80.3; H, 7.3; N, 7.8.

^1H NMR (400 MHz, CDCl3) δ_H 8.43 (1H, d, *J* 2.9), 8.12 (1H, dd, *J* 0.5, 8.1), 8.09 (1H, d, *J* 7.5), 8.04 (1H, s), 7.79 (1H, d, *J* 8.7), 7.73 (1H, dd, *J* 8.2, 1.5), 7.45 (1H, td, *J* 8.1, 1.2), 7.40 (1H, d, *J* 8.1), 7.30 (1H, dd, *J* 8.7, 3.0), 7.21 (1H, td, *J* 7.9, 1.1), 4.36 (2H, t, *J* 7.4, NCH_2), 3.91 (3H, s, OCH_3), 1.94-1.84 (2H, m, NCH_2CH_2), 1.46-1.21 (6H, m), 0.84 (3H, t, *J* 7.1, CH_3).

^{13}C NMR (101 MHz, $CDCl_3$) δ_C 155.00, 151.32, 141.50, 141.34, 137.33, 137.14, 126.02, 123.19, 122.93, 121.69, 120.76, 120.70, 119.14, 117.77, 109.06, 106.99, 100.29, 56.03, 43.41, 31.91, 29.30, 27.28, 22.88, 14.33.

GC-MS (EI) *m/z* = 287 (M^+ - C_5H_{11}, 100%), 358 (M^+, 89).

Preparation of 9-hexyl-2-(4-methoxypyridin-2-yl)-9H-carbazole (73)

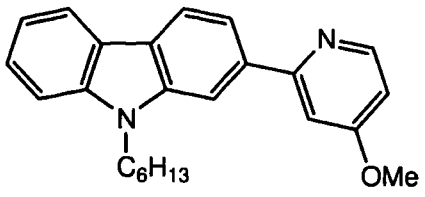

(73)

An argon-filled flask was charged with **60** (1.00 g, 3.39 mmol) which was dissolved in degassed toluene (150 ml). To this solution Na_2CO_3 solution (2 M, 4.13 g, 38.9 9mmol), tetrakis(triphenylphosphine)palladium(0) (0.25 g, 0.22 mmol) and 2-bromo-4-methoxypyridine (0.60 g, 3.17 mmol) were added. Following the procedure described for **70** gave a light yellow liquid as the crude product. This was purified by column chromatography on silica using an eluent of DCM:EtOAc (9:1 v/v) to give a clear yellow oil **73** (0.57 g, 49%). Upon adding the oil to hexane:EtOAc (2:1 v/v) **73** crystallised as shiny white crystals; mp 97-98 °C.

Found: C, 80.3; H, 7.3; N, 7.8. Calc. for $C_{24}H_{26}N_2O$: C, 80.3; H, 7.3; N, 7.8.

^{1}H NMR (400 MHz, $CDCl_3$) δ_H (8.56 (1H, d, *J* 5.7), 8.17-8.08 (3H, m), 7.76 (1H, dd, *J* 8.1, 1.4), 7.47 (1H, td, *J* 8.1, 1.0), 7.41 (1H, d, *J* 8.2), 7.36 (1H, d, *J* 2.4), 7.26-7.20 (1H, m), 6.78 (1H, dd, *J* 5.7, 2.4), 4.37 (2H, t, *J* 7.4, NCH_2), 3.93 (3H, s, OCH_3), 1.95-1.84 (2H, m, NCH_2CH_2), 1.45-1.36 (2H, m), 1.36-1.21 (4H, m), 0.84 (3H, t, *J* 7.1, CH_3).

^{13}C NMR (101 MHz, $CDCl_3$) δ_C 166.59, 160.24, 151.08, 141.47, 141.07, 137.26, 126.11, 123.76, 122.72, 120.77, 120.56, 119.08, 118.06, 109.02, 107.96, 107.61, 107.48, 55.36, 43.31, 31.79, 29.20, 27.15, 22.75, 14.20.

GC-MS (EI) *m/z* = 244 (100%), 287 (M^+ - C_5H_{11}, 56), 358 (M^+, 12).

Preparation of *fac*-{2-[5-(trifluoromethyl)pyridin-2-yl]-9-hexyl-9H-carbazole}$_3$Iridium^{III} (44)

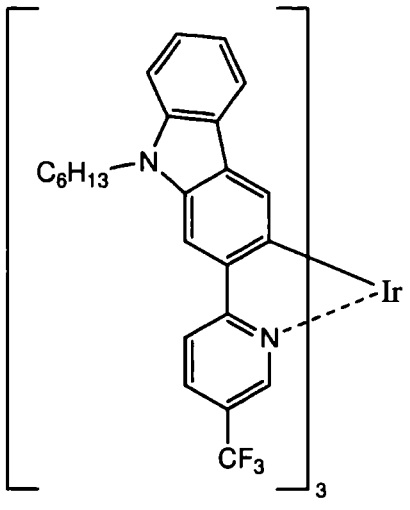

(**44**)

An argon-filled flask was charged with **69** (0.41 g, 1.03 mmol) and Ir(acetylacetonate)$_3$ (0.14 g, 0.29 mmol) which were dissolved in degassed glycerol (15 ml). The solution was heated at 220 °C for 65 h. After this time the solution was allowed to cool to room temperature and was diluted with distilled H_2O (50 ml) and brine solution. The organic products were extracted with DCM (4x30 ml) and dried ($MgSO_4$). The solvent was removed *in vacuo* to give a dark red liquid as the crude product. This was purified by column chromatography on silica using petroleum ether:DCM (3:1 v/v) to give **44** (0.01 g, 1%) as a dark red powder.

^{1}H NMR (500 MHz, CD_2Cl_2) δ_H 8.25 (3H, d, *J* 9.3), 7.90-7.86 (9H, m), 7.50 (3H, d, *J* 7.8), 7.43 (3H, s), 7.34-7.27 (6H, m), 6.87-6.84 (3H, m,), 4.33 (6H, t, *J* 7.4, NCH_2), 1.98-1.87 (6H, m), 1.46-1.29 (18H, m), 0.88 (9H, t, *J* 7.2, CH_3).

^{13}C NMR (126 MHz, CD_2Cl_2) δ_C 171.50, 148.54, 144.74, 142.29, 140.32, 137.75, 133.84, 128.01, 127.76, 126.45, 124.72, 123.64, 122.33, 121.53, 119.55, 118.34, 108.77, 107.01, 43.50, 32.23, 29.48, 27.59, 23.18, 14.38.

MS (MALDI-TOF) *m/z* = 1378 (M^+, 100%).

Preparation of *fac*-{2-[4-(trifluoromethyl)pyridin-2-yl]-9-hexyl-9H-carbazole}$_3$Iridium^{III} (45)

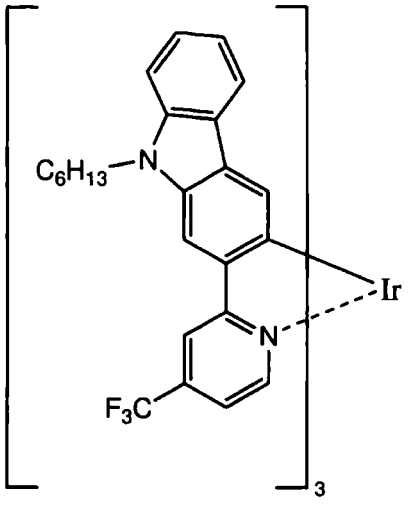

(**45**)

An argon-filled flask was charged with **71** (0. 41g, 1.02 mmol) and Ir(acetylacetonate)$_3$ (0.15 g, 0.31 mmol) which were dissolved in degassed glycerol (15 ml). Following the procedure described for **44** gave a dark red liquid as the crude product. This was purified by column chromatography on silica using petroleum ether:DCM (3:1 v/v) to give **45** (0.03 g, 2%) as a dark red powder.

Found: C, 63.35; H, 5.2; N, 5.65. Calc. for $C_{72}H_{66}F_9IrN_6$: C, 62.7; H, 4.8; N, 6.1.

^{1}H NMR (500 MHz, CD_2Cl_2) δ_H 8.31 (3H, s), 7.88-7.89 (6H, m), 7.49 (3H, d, *J* 7.9), 7.40 (3H, s), 7.31-7.29 (6H, m), 7.08 (3H, d, *J* 5.5), 6.87-6.84 (3H, m), 4.34 (6H, t, *J* 7.1, NCH_2), 1.97-1.88 (6H, m, NCH_2CH_2), 1.49-1.22 (18H, m), 0.88 (9H, t, *J* 7.1, CH_3).

^{13}C NMR (126 MHz, CD_2Cl_2) δ_C 169.34, 148.87, 147.93, 142.17, 140.61, 138.12, 137.72, 127.84, 124.67, 126.30, 123.59, 122.38, 121.43, 118.33, 118.12, 115.68, 108.88, 106.19, 43.46, 32.26, 29.50, 27.54, 23.17, 14.39.

MS (MALDI-TOF) *m/z* = 1379 (M^+, 100%).

Preparation of *fac*-{9-hexyl-2-[5-methoxypyridin-2-yl]-9H-carbazole}$_3$Iridium^{III} (46)

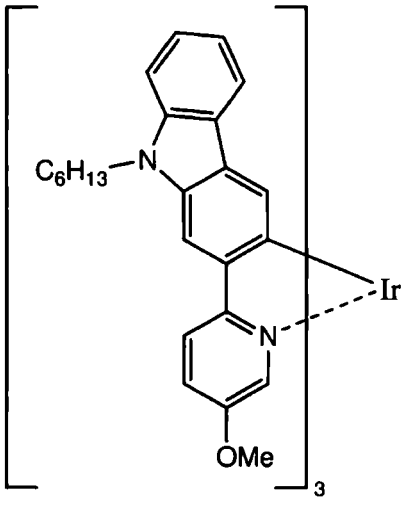

(46)

An argon-filled flask was charged with **72** (0.30 g, 0.84 mmol) and Ir(acetylacetonate)$_3$ (0.13 g, 0.26 mmol) which were dissolved in degassed glycerol (15 ml). Following the procedure described for **44** gave an orange liquid as the crude product. This was purified by column chromatography on silica using hexane:DCM (2:1 v/v) to give **46** (0.08 g, 8%) as a bright orange powder.

Found: C, 68.3; H, 6.0; N, 6.6. Calc. for $C_{72}H_{75}IrN_6O_3$: C, 68.4; H, 6.0; N, 6.7.

^{1}H NMR (500 MHz, CD_2Cl_2) δ_H 8.04 (3H, d, *J* 9.1), 7.69 (3H, s), 7.49 (3H, d, *J* 7.8), 7.37 (3H, d, *J* 2.7), 7.28-7.22 (12H, m), 6.82-6.76 (3H, m), 4.42-4.33 (6H, m, NCH_2), 3.66 (9H, s, OCH_3), 1.96-1.88 (6H, m, NCH_2CH_2), 1.47-1.42 (6H, m), 1.41-1.25 (12H, m), 0.88 (9H, t, *J* 7.2, CH_3).

^{13}C NMR (126 MHz, CD_2Cl_2) δ_C 160.37, 155.64, 145.69, 143.09, 141.18, 138.21, 135.45, 127.83, 125.24, 125.04, 122.96, 121.09, 121.00, 119.99, 117.99, 108.58, 103.86, 56.07, 43.15, 32.28, 29.89, 27.60, 23.19, 14.42.

MS (MALDI-TOF) *m/z* = 1265 (M^+, 100%).

Attempted preparation of *fac*-{9-hexyl-2-[4-methoxypyridin-2-yl]-9H-carbazole}$_3$Iridium^{III} (47)

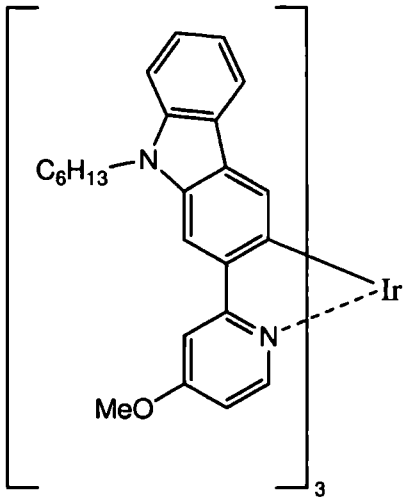

(47)

An argon-filled flask was charged with **73** (0.30 g, 0.86 mmol) and Ir(acetylacetonate)$_3$ (0.12 g, 0.25 mmol) which were dissolved in 15ml of degassed glycerol (15 ml) . Following the procedure described for **44** gave a dark oil which was a multi-component mixture as judged by TLC observations. The desired product **47** could not be isolated.

Chapter 4 – Conclusion

The aim of this work was to synthesise functionalised iridium complexes based on carbazole-pyridyl ligands for studies into the optical properties of the complexes and use in preliminary OLED devices. This aim has been achieved in the form of two series of iridium complexes totalling six new complexes with either an electron withdrawing or electron donating group on the pyridyl moiety in the complex. A number of synthetic routes to the complexes were explored although the highest yielding was found to be the previously published route by the Bryce group in the synthesis of the parent complexes.

The functionalisation of the complexes aimed to achieve a significant shift in emission wavelength of the complexes in relation to their parent complexes. The addition of the substituent group and the subsequent investigation of the optical properties of the complexes have lead to some interesting observations. The fluorescence emission maxima of the complexes in solution exhibit a large range in wavelengths spanning 123 nm covering green to red emission achieving the aim of tuning the emission colour. Preliminary studies on the incorporation of the complexes into OLED devices demonstrated low external quantum efficiencies, possibly due to a lower energy partially non-emissive excited state formed through interaction with the substituent group or poor transfer of excitons between the host and the guest complexes in the device.

The commercialisation of these complexes based on the current devices is unlikely due to the low external quantum efficiencies. As a study of the effect of substituent groups on the emission of a series of complexes this work has been very successful, with the application of this knowledge and an improved device structure these complexes could become attractive OLED components.

Chapter 5 – References

[1] Organic Light Emitting Diode (OLED) Displays – A Global Strategic Business Report, *Global Industry Analysts, Inc.*, 2008.

[2] H. J. Round, *Electr. World*, 1907, **49**, 308.

[3] N. Zheludev, *Nature Photonics*, 2007, **1**, 189.

[4] M. A. Baldo, D. F. O'Brien, M. E. Thompson, S. R. Forrest, *Phys. Rev. B*, 1999, **60**, 14422.

[5] C. Rothe, S. M. King, A. P. Monkman, *Phys. Rev. Lett.*, 2006, **97**, 076602.

[6] M. A. Baldo, D. F. O'Brien, Y. You, A. Shoustikov, S. Sibley, M. E. Thompson, S. R. Forrest, *Nature*, 1998, **395**, 151.

[7] P. S. Vincett, W. A. Barlow, R. A. Hann, G. G. Roberts, *Thin Solid Films*, 1982, **94**, 171.

[8] C. W. Tang, S. A. VanSlyke *Appl. Phys. Lett.*, 1987, **51**, 913.

[9] J. Kido, Y. Iizumi, *Chem. Lett.*, 1997, **26**, 963.

[10] C. Adachi, S. Tokito, T. Tsutsui, S. Saito, *Jpn. J. Appl. Phys.*, 1988, **27**, L269.

[11] S. A. Vanslyke, C. H. Chen, C. W. Tang, *Appl. Phys. Lett.*, 1996, **69**, 2160.

[12] J. H. Burrows, D. D. C. Bradley, A. R. Brown, R. N. Marks, K. Mackay, R. H. Friend, P. L. Burns, A. B. Holmes, *Nature*, **1990**, 347, 539.

[13] W. Helfrich, W. G. Schneider, *Phys. Rev. Lett.*, 1965, **14**, 229.

[14] H. Kallman, M. Pope, *J. Chem. Phys.*, 1959, **32**, 300.

[15] P. Mark, W. Helfrich, *J. Appl. Phys.*, 1962, **33**, 205.

[16] J. Kalinowski, J. Godlewski, Z. Dreger, *Appl. Phys. A*, 1985, **37**, 179.

[17] C. Adachi, S. Tokito, T. Tsutsui, S. Saito, *Jpn. J. Appl. Phys.*, 1988, **27**, L713.

[18] C. W. Tang, S. A. Vanslyke, C. H. Chen, *J. Appl. Phys.*, 1989, **65**, 3610.

[19] S. Hoshino, H. Suzuki, *Appl. Phys. Lett.*, 1996, **69**, 224.

[20] D. B. Papkovsky, *Sensors and Actuators B*, 1995, **29**, 213.

[21] M. S. Lowry, S. Bernhard, *Chem. Eur. J.*, 2006, **12**, 7970.

[22] Z. Kafafi, *Organic Electroluminescence*, Taylor & Francis Group, 2005, Boca Ranton.

[23] M. A. Baldo, S. Lamansky, P. E. Burrows, M. E. Thompson, S. R. Forrest, *Appl. Phys. Lett.*, 1999, **75**, 4.

[24] V. V. Grushin, N. Herron, D. D. LeCloux, W. J. Marshall, V. A. Petrov, Y. Wang, *Chem. Comm.*, 2001, 1494.

[25] P. J. Hay, *J. Phys. Chem. A*, 2002, **106**, 1634.

[26] J. Brooks, Y. Babayan, S. Lamansky, P. I. Djurovich, I. Tsyba, R. Bau, M. E. Thompson, *Inorg. Chem.*, 2002, **41**, 3055.

[27] S. Lamansky, P. Djurovich, D. Murphy, F. Abdel-Razzaq, H. Lee, C. Adachi, P. E. Burrows, S. R. Forrest, M. E. Thompson, *J. Am. Chem. Soc.*, 2001, **123**, 4304.

[28] Y. Kawamura, S. Yanagida, S. R. Forrest, *J. Appl. Phys., 2002, **92**,* 87.

[29] V. Adamovich, J. Brooks, A. Tamayo, A. M. Alexander, P. I. Djurovich, B. W. D'Andrade, C. Acachi, S. R. Forrest, M. E. Thompson, *New J. Chem.*, 2002, **26**, 1171.

[30] B. D'Andrade, J. Brooks, V. Adamovich, M. E. Thompson, S. R. Forrest, *Adv. Mater.*, 2002, **14**, 1032.

[31] H. A. Al-Attar, A. P. Monkman, M. Tavasli, S. Bettington, M. R. Bryce, *Appl. Phys Lett.*, 2005, **86**, 121101.

[32] A. B. Tamayo, B. D. Alleyne, P. I. Djurovich, S. Lamansky, I. Tsyba, N. N. Ho, B. Bau, M. E. Thompson, *J. Am. Chem. Soc.*, 2003, **125**, 7377.

[33] M. Tavasli, S. Bettington, M. R. Bryce, A. S. Batsanov, A. P. Monkman, *Synthesis*, 2005, 1619.

[34] S. Bettington, M. Tavasli, M. R. Bryce, A. Beeby, H. Al-Attar, A. P. Monkman, *Chem. Eur. J.*, 2007, **13,** 1423.

[35] W. Wong, C. Ho, Z. Gao, B. Mi, C. Chen, K. Cheah, Z. Lin, *Angew. Chem. Int. Ed.*, 2006, **45**, 7800; correction published *Angew. Chem. Int. Ed.*, 2007, **46**, 1558.

[36] Y. Tao, Q. Wang, K. Zhang, Q. Wang, T. Zou, J. Qin, D. Ma, *J. Mat. Chem.*, 2008, **18**, 4091.

[37] M. P. Krahl, A. Jäger, T. Krause, H. Knölker, *Org. Biomol. Chem.*, 2006, **4**, 3215

[38] B. Åkermark, L. Eberson, E. Jonsson, E. Pettersson, *J. Org. Chem.*, 1975, **40**, 1365

[39] A. Tsuboyama, H. Iwawaki, M. Furugori, T. Mukaide, J. Kamatani, S. Igawa, T. Moriyama, S. Miura, T. Takiguchi, S. Okada, M. Hoshino, K. Ueno, *J. Am. Chem. Soc.*, 2003, **125**, 12971

[40] N. G. Connelly, W. E. Geiger, *Chem. Rev.*, 1996, **96**, 877

[41] J. Li, P. I. Djurovich, B. D. Alleyne, M. Yousufuddin, N. N. Ho, J. C. Thomas, J. Peters, R. Bau, M. E. Thompson, *Inorg. Chem.*, 2005, **44**, 1713

[42] M. J. Frisch, G. W. Trucks, H. B. Schlegel, G. E. Scuseria, M. A. Robb, J. R. Cheeseman, J. A. Montgomery Jr., T. Vreven, K. N. Kudin, J. C. Burant, J. M. Millam, S. S. Iyengar, J. Tomasi, V. Barone, B. Mennucci, M. Cossi, G. Scalmani, N. Rega, G. A. Petersson, H. Nakatsuji, M. Hada, M. Ehara, K. Toyota, R. Fukuda, J. Hasegawa, M. Ishida, T. Nakajima, Y. Honda, O. Kitao, H. Nakai, M. Klene, X. Li, J. E. Knox, H. P. Hratchian, J. B. Cross, C. Adamo, J. Jaramillo, R. Gomperts, R. E. Stratmann, O. Yazyev, A. J. Austin, R. Cammi, C. Pomelli, J. W. Ochterski, P. Y. Ayala, K. Morokuma, G. A. Voth, P. Salvador, J. J. Dannenberg, V. G. Zakrzewski, S. Dapprich, A. D. Daniels, M. C. Strain, O. Farkas, D. K. Malick, A. D. Rabuck, K. Raghavachari, J. B. Foresman, J. V. Ortiz, Q. Cui, A. G. Baboul, S. Clifford, J. Cioslowski, B. B. Stefanov, G. Liu, A. Liashenko, P. Piskorz, I. Komaromi, R. L. Martin, D. J. Fox, T. Keith, M. A. Al-Laham, C. Y. Peng, A. Nanayakkara, M. Challacombe, P. M. W. Gill, B. Johnson, W.

Chen, M. W. Wong, C. Gonzalez, J. A. Pople, GAUSSIAN 03, Revision C.02, Gaussian Inc., Wallingford, CT, 2004.

[43] A. D. Becke, *J. Chem. Phys.*, 1993, **98**, 5648.

[44] C. Lee, W. Yang, R. G. Parr, *Phys. Rev. B*, 1988, **37**, 785.

[45] A. D. Becke, *Phys. Rev. A*, 1988, **38**, 3098.

[46] J. P. Perdew, *Phys. Rev. B*, 1986, **33**, 8822.

[47] G. A. Petersson, M. A. Al-Laham, *J. Chem. Phys.*, 1991, **94**, 6081.

[48] G. A. Petersson, A. Bennett, T. G. Tensfeldt, M. A. Al-Laham, W. A. Shirley, J. Mantzaris, *J. Chem. Phys.*, 1988, **89**, 2193.

[49] S. D. Kuduk, R. M. DiPardo, M. G. Bock, *Org. Lett.*, 2005, **7**, 577.